Development of Empirical Estimators for Feedback Control of Axisymmetric Jets

Aniruddha Sinha,[*] Andrea Serrani[†] and Mo Samimy[‡]

Gas Dynamics and Turbulence Laboratory, The Ohio State University, Columbus, OH, 43235

Localized arc filament plasma actuators have demonstrated significant potential in controlling high-speed and high Reynolds number axisymmetric jets in open-loop. As a first step in incorporating feedback for this control system, the authors have recently developed an empirical reduced-order model of the essential flow dynamics in the unforced jet using Proper Orthogonal Decomposition and Galerkin Projection. Real-time flow state estimation is a challenging problem in the implementation of feedback control for the complex flows of practical interest. Sensing the pressure in the irrotational near-field offers a suitable non-intrusive real-time measurement that is driven by the jet's shear layer dynamics. Several strategies are developed herein for estimating the state of the reduced-order model from pressure information. As in the dynamic modeling phase, the estimators are implemented and assessed on an existing direct numerical simulation database of an unforced jet similar to the experimental configuration. A linear time-varying Kalman filter is demonstrated to be more accurate than a single-time quadratic stochastic estimator when a single azimuthal array of pressure sensors is used. A single-time linear stochastic estimator is shown to be unsuitable for this problem. The fidelity of a linear time-invariant filter, that is only as complex as the linear stochastic estimator, is found to be comparable to the time-varying filter. Surprisingly, an extended Kalman filter that allows for a quadratic coupling between the state and output is found to under-perform the linear filter, possibly due to incorrect tuning.

Nomenclature

c_{EKF}	Constant output parameter for extended Kalman filter
c_{QSE}	Constant parameter for QSE
$\hat{e}_\alpha$	Figure of merit for estimation fidelity of POD modal coefficients
$\mathbf{l}_{EKF}$	Linear output parameter vector for extended Kalman filter
$\mathbf{l}_{LSE}$	LSE parameter vector
$\mathbf{l}_{QSE}$	Linear parameter vector for QSE
k	Time index
m	Azimuthal Fourier mode index
n	POD mode index
p	Fluctuating pressure
s	Pressure ring array index
$E()$	Expectation operator
$\mathbf{F}$	Linear state-transition matrix in discrete-time domain
K	Gain in Kalman filtering
$\mathbf{L}_{KF}$	Linear output parameter matrix for linear Kalman filter
N_m	Highest azimuthal Fourier mode retained
N_n	Highest POD mode retained

---

[*]Graduate Student, Dept. of Mechanical Engineering, AIAA Student Member.

[†]Associate Professor, Dept. of Electrical and Computer Engineering, AIAA Member.

[‡]The Howard D. Winbigler Professor of Engineering, Dept. of Mechanical Engineering, AIAA Fellow, Corresponding author, samimy.1@osu.edu

American Institute of Aeronautics and Astronautics

N_p	Number of axially distributed azimuthal ring arrays of pressure sensors
$\mathbf{Q}_{EKF}$	Quadratic output parameter matrix for extended Kalman filter
$\mathbf{Q}_{QSE}$	Quadratic parameter matrix for QSE
$\mathcal{X}_p$	Set of axial coordinates of azimuthal ring arrays of pressure sensors
α	POD modal coefficient
ζ	Normalized correlation coefficient
η	Uncertainty in state equation
κ	Uncertainty in linear output equation
ς	Uncertainty in quadratic output equation
Λ	POD eigenvalue
Ξ	Covariance matrix of uncertainty in linear output equation
Υ	Covariance matrix of uncertainty in state equation
Ψ	Covariance matrix of uncertainty in quadratic output equation
$()^i$	Imaginary part
$()^r$	Real part
$()^{\mathrm{T}}$	Transpose
$()^*$	Complex conjugate transpose
$\hat{()}$	Azimuthal Fourier transform
$\check{()}$	Extended Kalman filter variables that address all azimuthal modes
$\tilde{()}$	Estimated value

I.   Introduction

The work presented here is an integral module of a larger effort devoted to controlling a highly turbulent axisymmetric jet. The objectives are two-fold: mitigation of the noise propagating to the far-field, *or*, enhancement of the bulk mixing to hasten dissipation. In either case, the large-scale structures in the region of the shear-layer near the end of the potential core must be manipulated.[1,2] Over the past several years, localized arc filament plasma actuators (LAFPAs) have been developed in the Gas Dynamics and Turbulence Lab (GDTL) at The Ohio State University. These actuators have demonstrated considerable control authority on the said large-scale structures in open-loop control experiments.[3-5] As in any control system, the performance of the LAFPAs in open-loop is a function of the jet operating conditions, which are subject to variations and uncertainties. Thus, a natural advancement towards practical implementation is to incorporate feedback control, which may guarantee robustness in the presence of such uncertainties.

A simple feedback control strategy is *model-free* extremum-seeking control. Several variants of this idea were developed and successfully implemented for the lab-scale jet in GDTL.[6] However, since the dynamics of the system are ignored in a model-free controller, the responsiveness of the control system is limited. For improved responsiveness, a *model-based* controller is required that explicitly accounts for the dynamics. A necessary first step in this approach is to model the dynamics of the system *without* any actuation.

The authors proposed a strategy for educing such a baseline dynamical model from experimental data for the control system under consideration here.[7] In that work, a well-established direct numerical simulation (DNS) database[8] was employed for model development and validation. Two different models were created. The first model employed empirical data from the database directly, and served as a benchmark. The second model employed a reduced database that was created by mimicking the practical constraints that would be posed by actual experiments. The simulated trajectories of both models were compared back to the original database, and the fidelity was deemed sufficient for the purposes of feedback control. It is worth mentioning here that an assumption of incompressibility was shown to be valid for the control-oriented modeling of this high-speed jet. In the present work, the first model would be employed, and thus it is briefly described below along with some background information.

An incompressible flow is uniquely determined by specifying the three components of velocity over the entire flow domain. Considering compressibility effects, two additional thermodynamic variables are needed for a full characterization of the flow. In control system terminology, this information constitutes the set of *states* of the system. Since the dynamics of these states are governed by the infinite-dimensional Navier-Stokes equations, infinitely many states are needed to fully specify the flow. Such a model is not useful for practical control implementation, and one pursues model-reduction strategies instead. In developing a reduced-order model (ROM), a change of coordinates is sought such that a small set of the new coordinates

American Institute of Aeronautics and Astronautics

is required to approximately represent the original system. Proper Orthogonal Decomposition (POD) is the method of choice for reducing the order of flow kinematics using empirical data.[9–11] With this technique, the flow variables are projected onto the subspace spanned by the orthonormal spatial POD basis, and the new set of coordinates are the projection coefficients, also known as POD modal coefficients. Subsequently, one typically employs Galerkin Projection (GP) to obtain the dynamics of the flow in these new coordinates.[11] This route was adopted by the authors in developing the dynamical model under discussion.[7]

Feedback control of a system requires real-time observation of the state of the system, which is rarely feasible. Instead, one typically must resort to estimating the state from a related *output* variable that can be measured. To control an incompressible jet, its instantaneous velocity field must be available to the controller. Real-time measurement of the velocity in a high-speed jet is not feasible. However, this velocity field is strongly correlated with the pressure in the irrotational near-field of the jet.[2, 12–17] The latter can be acquired in real-time relatively non-intrusively, and being a scalar variable it is also easier to measure.[16] Thus, a more practical feedback control system would measure the pressure in the irrotational near-field in real-time, and use it to estimate the velocity.

State estimation for closed-loop control is essentially a filtering operation. As such, it may be divided into the following categories.

(a) The zero-memory, or single-time, variant involves using the measured output at each instant to directly estimate the state at that particular instant. This is the original form of stochastic estimation (SE), in which the state-output relation is determined by curve-fitting.

(b) The limited-memory estimation employs a finite backward-extended time history of outputs to approximate the state at any instant. This is the finite impulse response (FIR) filter, or the multi-time SE.

(c) In the infinite-memory variant, the entire history of outputs measured up to a point in time is used for the estimation of the state at that time; this is the infinite impulse response (IIR) filter. The linear time-invariant filter (LTIF) and Kalman filter (KF) are popular members of this category.

Stochastic estimation was originally introduced to educe coherent structures in turbulent flows.[18] Subsequently, this technique has also been employed for estimating flow variables using minimal measurements and a knowledge of the spatial correlations in the flow. The earliest implementations were of *linear* SE (LSE) in the areas of isotropic turbulence,[19] boundary layer,[20] and axisymmetric jet shear layer.[21] In these works, the instantaneous velocity at various locations in the flow were approximated as separate linear functions of the velocities measured at the same instant at only a few locations. In a parallel development, higher-order SE (HOSE), including quadratic SE (QSE), were implemented for isotropic turbulence,[22, 23] and the boundary layer.[20] These studies generally concluded that, compared to LSE, the marginal improvements in accuracy of estimation with HOSE did not warrant the added complications of computing the higher statistical moments.

Numerous researchers have advanced the original technique of SE in several significant directions. Instead of using measurements of the spatially-sparse velocity field itself to estimate a spatially-denser velocity field, measurements of other relevant flow quantities, viz. pressure and wall shear stress, have been used.[13, 24–31] This modification typically reduces the complexity of experiments since time-resolved velocity measurements are difficult and intrusive. As the formal solution of Poisson's equation indicates, the pressure field is related to the global velocity field. This implies that pressure-velocity correlations are strong across greater distances compared to velocity-velocity correlations. In the investigations where surface pressure was used in the estimation, significant improvements in accuracy were observed with QSE compared to LSE.[24, 25, 29, 30] For the application to the turbulent boundary layer, Naguib et al.[24] showed that this outcome indicates the comparable relevance of the mean-turbulent and turbulent-turbulent pressure source terms. Murray and Ukeiley[25] posited that the higher order terms were necessary since the linear model becomes less accurate when the measurement location is far away from the estimation location in the cavity flow configuration.

Another development of SE is its coupling with POD to obtain a *low-dimensional* estimate of the flow kinematics. In the classical version of the *complementary* technique, the velocity field obtained through LSE was further filtered using POD.[32, 33] In the *modified complementary* SE, first the POD modal coefficients of the velocity field were estimated using a different flow variable, say the pressure or wall shear stress, followed by a POD reconstruction of the velocity field from these estimates.[13, 16, 26, 27, 29, 30, 34] The concept was later extended by decomposing both the measured field and the field to be estimated into their respective low-dimensional spatial modes, be they Fourier and/or POD, before linking the corresponding modal coefficients

American Institute of Aeronautics and Astronautics

through stochastic estimation.[16, 35] The successive modifications were implemented to take advantage of the implicit spatial filtering and the increased correlations between the low-dimensional quantities, while reducing computations.

The above discussion focused on the single-time version of SE. In *single-time delay* SE, a delayed version of the measurement is used to estimate the field at any given time.[20, 24] This is useful where the time scales of the measurement and estimate are alike, but a fixed pre-determined convective delay has to be considered. On the other hand, *multi-time* SE uses measurements over a finite moving window stretching back in time for estimating the present state.[29, 36] This accounts for convection effects in the flow, while also taking advantage of the temporal persistence of the large-scale structures being estimated. Durgesh and Naughton[36] demonstrated that although the accuracy of estimation first improves with the size of the time window, the fidelity actually degrades quite rapidly beyond a certain size. Thinking from the perspective of polynomial curve-fitting, this may be explained by the over-determination of the fit of a high-degree polynomial in the absence of enough independent realizations. In real-time estimation, the number of delays in discrete time that can be considered is typically limited by hardware constraints.

Extending the concept of multi-time SE to the limit of theoretically infinite time, one arrives at the *spectral* variant of SE. This technique may be implemented for statistically stationary flows where the correlation is computed in the temporal Fourier domain.[16, 28, 33, 35] Tinney et al.[28] argued that the spectral SE is especially useful whenever the spectral features of the measured and estimated variables are disparate, and/or significant time delays exist between them.[28] In practical implementations, one is typically limited to a finite time window, but this has to be long enough for satisfactory resolution of the frequency content. Moreover, its non-recursive nature and the necessity of computing the temporal Fourier transform, restrict the spectral SE to offline estimation.

The above discussion indicates the need for a recursive filtering technique that would address the dynamics of the flow while avoiding the hardware constraints of limited memory. This is the essence of an IIR filter like the Kalman filter.[37–39] However, unlike SE, the KF needs a model of the flow dynamics. Such a model is precisely the ROM discussed above. One of the advantages of a model-based filter over a stochastic estimator is the inherent noise-filtering properties of the former.[40] In essence, by incorporating some predictive knowledge of the system, model-based filters may separate the noise from the signal. On the other hand, stochastic estimators typically pass through the unfiltered measurement noise to the state estimate. A different model-based technique is adjoint-based model predictive estimation.[40] Typically, this strategy is quite computation-intensive, and hence may not be as suitable for real-time control implementation as a Kalman filter.

Owing to the need for a reduced-order model of the flow dynamics, implementing a model-based state estimation is a challenge. Two recent contributions in this field are documented in Ref. 41, 42, where the used of Kalman filters has been proposed to estimate the full state of a channel flow, given spatially-resolved measurements of the two-component wall shear stress and wall pressure everywhere on the surfaces. Previously, it had been shown that a theoretically complete information of the flow can be deduced from this set of measurements.[40] Such comprehensive measurements are rarely feasible in unbounded flows, and one has to settle for far greater approximations. The present work proposes effective strategies in such a challenging situation.

Picard and Delville[13] were the first to use the irrotational near-field pressure to estimate the velocity in the axisymmetric jet shear layer with LSE. They employed a linear array of microphones aligned with the outer edge of the shear layer, and measured the axial and radial velocities simultaneously with a radial hot-wire rake. Later, Kastner et al.[31] used a similar microphone setup but measured the velocity using 2-component particle image velocimetry (PIV) in a meridional plane. They demonstrated that QSE substantially improves the estimation of the turbulent kinetic energy. Recently, Tinney et al.[16] measured the pressure on an azimuthal ring array of pressure transducers and used stereo-PIV on cross-stream slices, to implement the spectral linear SE. The present work builds on these techniques, but with a focus on real-time state estimation. The two main contributions of this article are the incorporation of a Kalman filter for infinite-memory estimation, and a multi-point single-time QSE in the Fourier azimuthal domain, both in the context of a jet shear layer.

A very useful (and, in fact, indispensable) tool for evaluating the various estimation strategies is a time- and spatially-resolved 3D volumetric database of the axisymmetric jet. Freund[8] has performed a direct numerical simulation (DNS) of an unforced Mach 0.9 axisymmetric jet with Reynolds number based on jet diameter (Re) of 3600. In spite of its low Reynolds number, most of its general characteristics, and especially
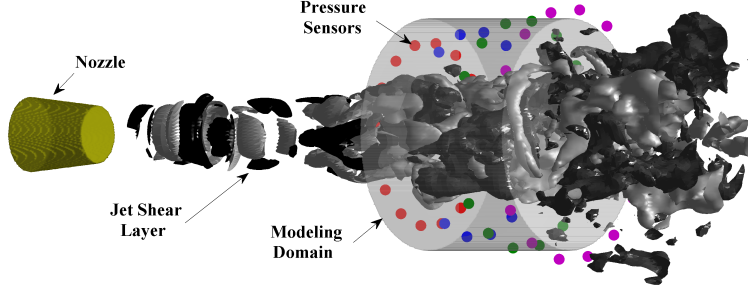
Figure 1. Schematic of the axisymmetric jet indicating the modeling domain and the model-state estimation strategy.

the nature of its large-scale structures, were found to be similar to those of a Mach 0.9 jet with an Re of 640,000 in an experiment.[43] This database was used to develop and validate the reduced-order modeling strategy in Ref. 7. In the present article, the DNS database is used to assess various strategies for estimating the state of the reduced-order model.

A brief review of the reduced-order model of the jet appears in Section II. The various strategies for real-time state estimation are laid out in Section III. These strategies are assessed in simulation, and the results are presented in Section IV. Concluding remarks are offered in Section V.

II.   Modeling of Jet Dynamics: A Review

The flow domain of the axisymmetric jet is unbounded; the first step in model order reduction is to choose a bounded region that is most pertinent for the control objectives at hand. An appropriate choice is a cylindrical domain covering the shear layer in the vicinity of the end of the potential core, as shown in Figure 1. A reduced-order dynamic model of the flow in this region was developed by the authors.[7] Before introducing the notation for this model, the relevant normalizations are established.

Let the jet exit velocity and nozzle exit diameter be U_{jet} and D, respectively. All velocities and linear coordinates are implicitly normalized by these respective quantities. Time is normalized by the flow time scale $t^+ := D/U_{jet}$. Pressure is normalized by $\rho_{jet} U_{jet}^2$, where ρ_{jet} is the jet exit density. With the kinematic viscosity of the jet at exit denoted by ν_{jet}, the pertinent Reynolds number is $Re := U_{jet}D/\nu_{jet}$.

Employing cylindrical coordinates $\mathbf{x} := (x, r, \theta)^{\mathrm{T}}$, the modeling domain is $\Omega := [X_1, X_2] \times [0, R] \times \mathbb{T}$. Here, X_1 and X_2 denote the upstream and downstream bounds of the axial domain, R is the radial extent of the measurement domain, and $\mathbb{T}$ is the circle group. The velocity vector is $\mathbf{U} : \Omega \times \mathbb{R} \to \mathbb{R}^3$, $\mathbf{U} : (\mathbf{x}, t) \mapsto (U_x, U_r, U_\theta)^{\mathrm{T}}$. The statistical stationarity and axisymmetry of the jet are used to define the mean velocity field as $\overline{\mathbf{U}}(x, r) := E\left\{ (1/2\pi) \int_{-\pi}^{\pi} \mathbf{U}(x, r, \theta, t) \mathrm{d}\theta \right\}$. Henceforth, unless otherwise mentioned, the expectation operator $E(\cdot)$ will signify the ensemble-average. Intuitively, $\overline{U}_\theta \approx 0$, and this is enforced explicitly in the implementation. The fluctuating velocity vector is defined as $\mathbf{u}(x, r, \theta, t) := \mathbf{U}(x, r, \theta, t) - \overline{\mathbf{U}}(x, r)$, with the three components being u_x, u_r, and u_θ, respectively.

The azimuthal direction is homogenous and periodic, so that any generic flow variable $w(\theta)$ lends itself to the azimuthal Fourier transform denoted by $w(\theta) \xrightarrow{\mathcal{F}_m} \hat{w}(m)$; $\hat{w}(m) := (1/2\pi) \int_{-\pi}^{\pi} w(\theta) \mathrm{e}^{-\mathrm{i}m\theta} \mathrm{d}\theta$. Here m is the azimuthal mode. The inverse Fourier transform will be denoted by $\hat{w}(m) \xrightarrow{\mathcal{F}_\theta} w(\theta)$; $w(\theta) = \sum_{m=-\infty}^{\infty} \hat{w}(m) \mathrm{e}^{\mathrm{i}m\theta}$. With this, $\mathbf{u}$ is transformed as $\mathbf{u}(x, r, \theta, t) \xrightarrow{\mathcal{F}_m} \hat{\mathbf{u}}(x, r, t; m)$. The highest azimuthal mode that can be resolved is limited by the azimuthal grid resolution. Moreover, typically the higher azimuthal modes are dynamically insignificant. So, in the remaining paper, the azimuthal modes would be taken in the truncated range $m \in [-N_m, N_m]$.

The fluctuating velocity field $\mathbf{u}(\cdot, t)$ belongs to the Hilbert space of square-integrable functions $\mathcal{L}_\Omega^2$ equipped with inner product denoted by $\langle \cdot , \cdot \rangle_\Omega$. The goal of POD is, given an ensemble of data for $\mathbf{u} \in \mathcal{L}_\Omega^2$, to find a subspace $S \subset \mathcal{L}_\Omega^2$ of fixed dimension N_n, such that the error $E\{\|\mathbf{u} - \mathcal{P}_S \mathbf{u}\|\}$ is minimized.[44] Here, $\|\cdot\|$ is the induced norm on $\mathcal{L}_\Omega^2$, and $\mathcal{P}_S$ is the orthogonal projection onto the subspace S. The details of POD have been well-established elsewhere.[9–11, 44, 45] For the purpose of the present discussion, it is sufficient to state that in the presence of the homogenous azimuthal direction, the POD devolves into the following

American Institute of Aeronautics and Astronautics

integral eigenvalue problem for each azimuthal mode $m \in [-N_m, N_m]$:[7]

$$\int_{X_1}^{X_2} \int_0^R E\left\{\hat{\mathbf{u}}(x,r,t;m)\hat{\mathbf{u}}^*(x',r',t;m)\right\} \hat{\mathbf{\Phi}}^{(n)}(x',r';m)r'\mathrm{d}r'\mathrm{d}x' = \Lambda^{(n)}(m)\hat{\mathbf{\Phi}}^{(n)}(x,r;m),$$

$$(x,r) \in [X_1, X_2] \times [0,R]. \tag{1}$$

The quantities Λ and $\hat{\mathbf{\Phi}}$ are respectively the eigenvalue and eigenfunction for the nth POD mode. The asterisk denotes the adjoint operation, which reduces to the complex-conjugate transpose for our purpose.

The POD mode number indexes the real non-negative eigenvalues in descending order. Then, the first N_n eigenfunctions form the desired optimal basis for the subspace S. This allows the following approximate change of coordinates for each azimuthal mode m:

$$\hat{\mathbf{u}}(x,r,t;m) \approx \sum_{n=1}^{N_n} \alpha^{(n)}(t;m)\hat{\mathbf{\Phi}}^{(n)}(x,r;m), \tag{2}$$

where, the nth POD modal coefficient is computed as

$$\alpha^{(n)}(t;m) = \int_{X_1}^{X_2} \int_0^R \hat{\mathbf{\Phi}}^{(n)*}(x,r;m)\hat{\mathbf{u}}(x,r,t;m)r\mathrm{d}r\mathrm{d}x. \tag{3}$$

The salient properties of the solutions of the POD problem have been discussed in depth elsewhere;[11,44] the following properties are the most germane to the ensuing discussion:

$$\alpha^{(n)}(t;-m) = \alpha^{(n)*}(t;m), \tag{4a}$$

$$E\left\{\alpha^{(n)}(t;m)\alpha^{(n')*}(t;m')\right\} = \Lambda^{(n)}(m)\delta_{m,m'}\delta_{n,n'}, \tag{4b}$$

where, δ is the Kronecker delta.

The above discussion focused on the reduced-order modeling of the flow kinematics; the dynamics will be considered next. The incompressible Navier-Stokes equation governing the flow can be formally written as $\dot{\mathbf{U}} = \mathcal{N}(\mathbf{U})$, where $\mathcal{N}$ is a vector field on $\mathcal{L}_\Omega^2$. The goal of reduced-order dynamics modeling is, given the finite-dimensional subspace S of $\mathcal{L}_\Omega^2$, to determine a dynamical system that evolves on S and approximates the original dynamics in some sense.[44] Galerkin Projection specifies the new vector field on S as the orthogonal projection of $\mathcal{N}$ onto S.

In Ref. 7, the authors showed that the application of GP to the axisymmetric jet results in the following set of coupled quadratic ODEs that govern the evolution of the POD modal coefficients

$$\dot{\alpha}^{(n)}(t;m) = \sum_{n'=1}^{N_n} f_{nn'}(m)\alpha^{(n')}(t;m),$$

$$+ (1 - \delta_{m,0}) \sum_{m'=m-N_m}^{N_m} \sum_{n',n''=1}^{N_n} g_{nn'n''}(m,m')\alpha^{(n')}(t;m')\alpha^{(n'')}(t;m-m'), \quad n \in [1,N_n], \ m \in [0,N_m]. \tag{5}$$

The time-independent coefficients f and g are determined from the POD eigenfunctions and the mean velocity profile $\overline{\mathbf{U}}$, both of which are extracted from the empirical database; the details appear in Ref. 7. It is important to note that although the POD modal coefficients are in the complex domain, f and g are real.[7] Furthermore, Eqn. (5) was only stated for the non-negative azimuthal Fourier modes by appealing to the Hermitian property in Eqn. (4a).

For model-based feedback control of the jet, Eqn. (5) represents the requisite reduced-order model of the dynamics in state-space form. It is clear that the POD modal coefficients constitute the state to be estimated in real-time.

The feedback control will be implemented in discrete time, hence the continuous dynamics must be converted to a sampled dynamical system. The appropriate sampling rate for the present implementation is the rate at which data was saved in the DNS database; this would be denoted by T_s. The sampled version of the state of the ROM is denoted by $\alpha_k^{(n)}(m) \equiv \alpha^{(n)}(t = kT_s; m)$, where $k \in \mathbb{N}$, the set of natural numbers. For each individual azimuthal mode, the state vector is defined as

$$\boldsymbol{\alpha}_k(m) := \begin{bmatrix} \alpha_k^{(1)}(m) & \cdots & \alpha_k^{(N_n)}(m) \end{bmatrix}^{\mathrm{T}} \in \mathbb{C}^{N_n}, \quad m \in [-N_m, N_m]. \tag{6}$$

American Institute of Aeronautics and Astronautics

III.   Estimator Modeling

Two main approaches are taken for real-time estimation of the state of the jet shear layer in Eqn. (5). In the first approach, single-time modified complementary stochastic estimation is used to directly estimate the POD modal coefficients as a function of the pressure measured in the irrotational near-field. This procedure does not utilize the known dynamics of the jet as captured by the model of Eqn. (5). Both linear and quadratic SE are evaluated. Alternatively, a Kalman filter is implemented that uses the derived ROM of the jet, as well as a static *output equation* that expresses the near-field pressure as a function of the POD modal coefficients at any instant of time. Both linear and quadratic output equations are investigated.

It is not trivial to obtain the said output equation from first principles. One option is to extend the incompressibility assumption made in the derivation of the ROM to argue for the approximate validity of Poisson's equation for pressure. Subsequently, one can explicitly solve this equation in real-time, as was done in Ref. 46. However, a viable alternative is to use stochastic estimation to derive this equation from empirical data. Note that this represents the inverse of the SE problem for single-time state estimation.

Consider N_p azimuthal arrays of pressure transducers arranged at different axial locations $x \in \mathcal{X}_p$, as seen in Figure 1. Without loss of generality, it is assumed that all pressure sensors are located on the surface of a virtual cone co-axial with the jet, so that their radial locations are a function of their axial locations. The individual pressure signals from the sensors in the azimuthal arrays are denoted as $P : \mathbb{T} \times \mathbb{R} \times [1, N_p] \to \mathbb{R}, \ P : (\theta, t; s) \mapsto \mathbb{R}$. In discrete time, the notation is $P_k(\theta; s) \equiv P(\theta, t = kT_s; s)$, where $k \in \mathbb{N}$. As before, the mean and fluctuating pressure are defined as $\overline{P}(s) := E\left\{(1/2\pi) \int_{-\pi}^{\pi} P_k(\theta; s) \mathrm{d}\theta\right\}$, and $p_k(\theta; s) := P_k(\theta, t; s) - \overline{P}(s)$, respectively. The azimuthal Fourier transform of p is defined in the usual manner: $p_k(\theta; s) \xrightarrow{\mathcal{F}_m} \hat{p}_k(s, m)$. Since $p_k(\theta; s)$ is real, $\hat{p}_k(s, m)$ is Hermitian in m. For each individual azimuthal mode, the output vector is defined as

$$\hat{\mathbf{p}}_k(m) := \left[\ \hat{p}_k(1, m) \quad \cdots \quad \hat{p}_k(N_p, m)\ \right]^{\mathrm{T}} \in \mathbb{C}^{N_p}, \quad m \in [-N_m, N_m]. \tag{7}$$

Before proceeding further, two remarks are in order; these will be cited repeatedly in the sequel.

Remark 1 *Since the jet is axisymmetric, the statistics should be independent of the direction of measurement of the azimuthal coordinate. The authors used this property to show that if a realization had a particular value of a POD modal coefficient, then one can* extend *the database by appending another realization where the value of the POD modal coefficient is its complex conjugate.[7] The same reasoning was invoked to argue that the two above realizations would have pressure signals that are also complex conjugates of each other. Following this reasoning, one can conclude that any order of statistical moment involving these quantities would be real, although the individual values are complex.*

Remark 2 *In the axisymmetric jet, the azimuthal direction is homogenous, and the stochastic estimation would be performed in the azimuthal Fourier domain for reasons mentioned earlier. The following well-established result is relevant in this discussion. Consider K arbitrary scalar fields in the azimuthal Fourier domain $\hat{\xi}_1$ to $\hat{\xi}_K$. Then, for azimuthal modes m_1 to m_K, their cumulative spectrum satisfies the relation*

$$E\left\{\hat{\xi}_1(m_1) \times \cdots \times \hat{\xi}_K(m_K)\right\} = \hat{\Pi}_{\xi_1, \cdots, \xi_K}(m_1, \cdots, m_K)\, \delta_{m_1 + \cdots + m_K, 0}.$$

In the above, $\hat{\Pi}_{\xi_1, \cdots, \xi_K}(m_1, \cdots, m_K)$ is the azimuthal Fourier transform of the corresponding cumulative correlation in the physical domain. In particular, this means that $\hat{\xi}_K(m_K)$ is only correlated to certain products of azimuthal modes of the remaining variables.

III.A.   Stochastic Estimation

III.A.1.   Linear Stochastic Estimation

The estimated version of any quantity w will be denoted by $\tilde{w}$. In the application of static LSE to the state estimation problem, the following relationship is posited

$$\tilde{\alpha}_k^{(n)}(m) = \mathbf{1}_{LSE}^{(n)*}(m)\hat{\mathbf{p}}_k(m), \quad n \in [1, N_n],\ m \in [0, N_m], \tag{8}$$

where, $\mathbf{l}_{LSE} \in \mathbb{C}^{N_p}$ represents the family of LSE parameter vectors. It is to be noted that, following Remark 2, the estimation problem for each azimuthal Fourier mode is decoupled.

For each $m-n$ pair, LSE proceeds by defining the mean square estimation error $E\left\{\left|\tilde{\alpha}_k^{(n)}(m) - \alpha_k^{(n)}(m)\right|^2\right\}$, which is quadratic in the respective parameter vector. The optimal parameter vector is located at the unique global minimum of the error surface; the expression is

$$\mathbf{l}_{LSE}^{(n)}(m) = E\left\{\hat{\mathbf{p}}_k(m)\hat{\mathbf{p}}_k^*(m)\right\}^{-1} E\left\{\hat{\mathbf{p}}_k(m)\alpha_k^{(n)*}(m)\right\}, \quad n \in [1, N_n], \ m \in [0, N_m]. \tag{9}$$

Following Remark 1, the estimation parameters can be concluded to be real.

III.A.2. *Quadratic Stochastic Estimation*

The most general quadratic function of the measured pressure for estimating any POD modal coefficient is

$$\tilde{\alpha}_k^{(n)}(m) = \delta_{m,0}c_{QSE}^{(n)*} + \mathbf{l}_{QSE}^{(n)*}(m)\hat{\mathbf{p}}_k(m) + \sum_{m'=m-N_m}^{N_m} \hat{\mathbf{p}}_k^{\mathrm{T}}(m')\mathbf{Q}_{QSE}^{(n)*}(m', m-m')\hat{\mathbf{p}}_k(m-m'),$$

$$n \in [1, N_n], \ m \in [0, N_m]. \tag{10}$$

Here, the family of constant, linear, and quadratic estimation parameters are respectively $c_{QSE} \in \mathbb{C}$, $\mathbf{l}_{QSE} \in \mathbb{C}^{N_p}$ and $\mathbf{Q}_{QSE} \in \mathbb{C}^{N_p \times N_p}$. Again, Remark 2 has been invoked to argue that the particular products of azimuthal Fourier modes of pressure considered above are the only ones that have non-vanishing correlations with the respective POD modal coefficients under consideration. Note that the estimator requires negative azimuthal Fourier modes of pressure, which can be retrieved from the Hermitian symmetry relation $\hat{\mathbf{p}}_k(-m') = \hat{\mathbf{p}}_k^*(m')$.

A review of the literature did not reveal any exposition of the implementation of QSE for multi-point measurements in a Fourier modal domain. Thus a generalized development is detailed in Appendix A. It is only noted here that, as in the LSE above, Remark 1 may be invoked to argue that all estimation parameters in Eqn. (10) are real.

III.B. Kalman Filtering

This work represents the first attempt at implementing a Kalman filter for estimating the state of a jet shear layer. To explore the applicability of such an approach, it was decided to begin with a linear system model. The trivial solution of the ROM in Eqn. (5) is an equilibrium point of the system. Linearizing about this point involves simply truncating the quadratic portion of the vector field. Note that this decouples the dynamics of the individual azimuthal modes.

Previously it has been pointed out that the filter needs to be implemented in a sampled-data system. Then, the following linearized model is obtained with the standard zero-order hold assumption:[47]

$$\boldsymbol{\alpha}_{k+1}(m) = \mathbf{F}(m)\boldsymbol{\alpha}_k(m) + \boldsymbol{\eta}_k(m), \quad m \in [0, N_m]. \tag{11}$$

Here, $\mathbf{F}(m) = \exp(\mathbf{F}_c(m)T_s)$, with the element in the nth row and n'th column of the real square matrix $\mathbf{F}_c(m)$ being $f_{nn'}(m)$ from Eqn. (5).[47] As is common in Kalman filtering, the uncertainties introduced by the modeling approximations, including the linearization, are addressed by the family of additive noise sequences $\boldsymbol{\eta} \in \mathbb{C}^{N_n}$, which are assumed to be stationary independent random processes (white noise) with identically zero mean and constant covariance matrices

$$E\left\{\boldsymbol{\eta}_k(m)\boldsymbol{\eta}_{k'}^*(m')\right\} = \boldsymbol{\Upsilon}(m)\delta_{k,k'}\delta_{m,m'}. \tag{12}$$

The matrices $\boldsymbol{\Upsilon}$ are real following Remark 1. Only the non-negative azimuthal modes are addressed in Eqn. (11) by appealing to Eqn. (4a).

III.B.1. *Linear Kalman Filtering*

The original KF was developed for a linear system.[37] The model of the state dynamics has already been linearized in Eqn. (11). The linear output equation specifies the measured pressure as a function of the state at every instant of time:

$$\hat{\mathbf{p}}_k(m) = \mathbf{L}_{KF}^*(m)\boldsymbol{\alpha}_k(m) + \boldsymbol{\kappa}_k(m), \quad m \in [0, N_m], \tag{13}$$

where, the family of parameters are $\mathbf{L}_{KF} \in \mathbb{C}^{N_n \times N_p}$. The decoupling of the azimuthal Fourier modes follows from Remark 2. The KF formalism models the measurement uncertainties by the family of additive sequences $\boldsymbol{\kappa} \in \mathbb{C}^{N_p}$ that are independent random processes (white noise) with identically zero means and constant covariance matrices

$$E\left\{\boldsymbol{\kappa}_k(m)\boldsymbol{\kappa}_{k'}^*(m')\right\} = \boldsymbol{\Xi}(m)\delta_{k,k'}\delta_{m,m'}. \tag{14}$$

The matrices $\boldsymbol{\Xi}$ are real from Remark 1. Additionally, it is commonplace to assume that the dynamic uncertainties appearing in Eqn. (11) are not correlated with the measurement uncertainties; i.e.,

$$E\left\{\boldsymbol{\eta}_k(m)\boldsymbol{\kappa}_{k'}^*(m')\right\} = \mathbf{0}. \tag{15}$$

In this preliminary attempt at implementing a KF for jet shear layer state estimation in real-time, the matrices $\mathbf{L}_{KF}$ would be determined using static modified complementary LSE discussed earlier in Section III.A.1. Appealing to the orthogonality of the POD modal coefficients from Eqn. (4b), the LSE yields

$$\mathbf{L}_{KF}(m) = E\left\{\boldsymbol{\alpha}_k(m)\boldsymbol{\alpha}_k^*(m)\right\}^{-1} E\left\{\boldsymbol{\alpha}_k(m)\hat{\mathbf{p}}_k^*(m)\right\} = \begin{bmatrix} \dfrac{E\left\{\alpha_k^{(1)}(m)\hat{\mathbf{p}}_k^*(m)\right\}}{\Lambda^{(1)}(m)} \\ \vdots \\ \dfrac{E\left\{\alpha_k^{(N_n)}(m)\hat{\mathbf{p}}_k^*(m)\right\}}{\Lambda^{(N_n)}(m)} \end{bmatrix}, \quad m \in [0, N_m]. \tag{16}$$

As before, Remark 1 is invoked to argue that the correlations appearing in the above expression are real, so that the parameter matrices $\mathbf{L}_{KF}$ are also real.

The notation and equations for the KF are adopted from Ref. 39. Denote the estimate of $\boldsymbol{\alpha}_{k+1}(m)$ given all measurements $\hat{\mathbf{p}}_{k'}(m)$ for $k' \in [0, k]$ by $\tilde{\boldsymbol{\alpha}}_{k+1/k}(m)$. Similarly, $\boldsymbol{\Gamma}_{k/k-1}(m)$ is the auto-covariance of estimation error at k given the measurements up to $k-1$, i.e.

$$\boldsymbol{\Gamma}_{k/k-1}(m) := E\left[\left\{\boldsymbol{\alpha}_k(m) - \tilde{\boldsymbol{\alpha}}_{k/k-1}(m)\right\}\left\{\boldsymbol{\alpha}_k(m) - \tilde{\boldsymbol{\alpha}}_{k/k-1}(m)\right\}^*\right].$$

Then, the following relations specify the Kalman Filter

$$\mathbf{K}_k(m) = \mathbf{F}(m)\boldsymbol{\Gamma}_{k/k-1}(m)\mathbf{L}_{KF}(m)\left(\mathbf{L}_{KF}^*(m)\boldsymbol{\Gamma}_{k/k-1}(m)\mathbf{L}_{KF}(m) + \boldsymbol{\Xi}(m)\right)^{-1}, \tag{17a}$$

$$\tilde{\boldsymbol{\alpha}}_{k+1/k}(m) = \mathbf{F}(m)\tilde{\boldsymbol{\alpha}}_{k/k-1}(m) + \mathbf{K}_k(m)\left(\hat{\mathbf{p}}_k(m) - \mathbf{L}_{KF}^*(m)\tilde{\boldsymbol{\alpha}}_{k/k-1}(m)\right), \tag{17b}$$

$$\boldsymbol{\Gamma}_{k+1/k}(m) = \left(\mathbf{F}(m) - \mathbf{K}_k(m)\mathbf{L}_{KF}^*(m)\right)\boldsymbol{\Gamma}_{k/k-1}(m)\left(\mathbf{F}(m) - \mathbf{K}_k(m)\mathbf{L}_{KF}^*(m)\right)^* + \boldsymbol{\Upsilon}(m)$$
$$+ \mathbf{K}_k(m)\boldsymbol{\Xi}(m)\mathbf{K}_k^*(m), \tag{17c}$$

$$\tilde{\boldsymbol{\alpha}}_{0/-1}(m) = \mathbf{0}, \tag{17d}$$

$$\boldsymbol{\Gamma}_{0/-1}(m) = \text{diag}\begin{pmatrix} \Lambda^{(1)}(m) & \cdots & \Lambda^{(N_n)}(m) \end{pmatrix}. \tag{17e}$$

The first equation defines the time-varying Kalman gain, whereas the second and third equations recursively propagate the state estimate and the state error covariance estimate, respectively. The fourth equation sets the initial condition for the state estimate to the zero vector, in the absence of any other information. Then, the initial condition for the error covariance in the fifth equation becomes equal to the covariance of the state vector itself. The latter is known to be the diagonal matrix of POD eigenvalues.

The state dynamics and output equations (see Eqns. (11) and (13)) are time-invariant, but the state model may not have a stable equilibrium. Then, Ref. 39 shows that the Kalman filter will be asymptotically stable if (a) the pairs $[\mathbf{F}(m), \mathbf{L}_{KF}^*(m)]$ are completely detectable, and (b) the pairs $[\mathbf{F}(m), \mathbf{G}_1(m)]$ are completely stabilizable for any $\mathbf{G}_1(m)$ such that $\mathbf{G}_1(m)\mathbf{G}_1^*(m) = \boldsymbol{\Upsilon}(m)$. The stationary (or steady-state) error-covariance matrices $\overline{\boldsymbol{\Gamma}}$ are obtained as solutions of the following set of decoupled discrete-time algebraic Riccati equations

$$\overline{\boldsymbol{\Gamma}}(m) = \mathbf{F}(m)\left[\overline{\boldsymbol{\Gamma}}(m) - \overline{\boldsymbol{\Gamma}}(m)\mathbf{L}_{KF}(m)\left(\mathbf{L}_{KF}^*(m)\overline{\boldsymbol{\Gamma}}(m)\mathbf{L}_{KF}(m) + \boldsymbol{\Xi}(m)\right)^{-1}\mathbf{L}_{KF}^*(m)\overline{\boldsymbol{\Gamma}}(m)\right]\mathbf{F}^*(m) + \boldsymbol{\Upsilon}(m). \tag{18}$$

The stationary Kalman gain matrix is obtained by inserting $\overline{\boldsymbol{\Gamma}}$ in Eqn. (17a). Use of stationary gains reduces the original time-varying KF to the linear time-invariant filter (LTIF). For this IIR filter, the only expression to be evaluated in real-time is Eqn. (17b), which is comparable in complexity to the LSE expression in Eqn. (8).

III.B.2. Extended Kalman Filtering

Instead of the linear output equation used in the KF above (see Eqn. (13)), one can posit the following set of quadratic output equations that mirrors Eqn. (10)

$$
\hat{p}_k(s,m) = \delta_{m,0} c^*_{EKF}(s) + \mathbf{l}^*_{EKF}(s,m)\boldsymbol{\alpha}_k(m) + \sum_{m'=m-N_m}^{N_m} \boldsymbol{\alpha}^{\mathrm{T}}_k(m')\mathbf{Q}^*_{EKF}(s,m',m-m')\boldsymbol{\alpha}_k(m-m')
$$
$$
+ \varsigma_k(s,m), \qquad s \in [1,N_p], \ m \in [0,N_m]. \tag{19}
$$

The specific coupling of the Fourier modes follows from Remark 2. The family of parameters are determined using QSE (see Appendix A). The parameters are real following Remark 1, i.e. $c_{EKF} \in \mathbb{R}$, $\mathbf{l}_{EKF} \in \mathbb{R}^{N_n}$, and $\mathbf{Q}_{EKF} \in \mathbb{R}^{N_n \times N_n}$. Also, the measurement uncertainties are modeled by the family of additive sequences $\varsigma \in \mathbb{C}$ that form the following vector

$$
\boldsymbol{\varsigma}_k(m) := \left[\ \varsigma_k(1,m) \quad \cdots \quad \varsigma_k(N_p,m) \ \right]^{\mathrm{T}} \in \mathbb{C}^{N_p}, \quad m \in [0,N_m]. \tag{20}
$$

These, in turn, are assumed to be independent random processes (white noise) with identically zero means and constant covariance matrices:

$$
E\left\{\boldsymbol{\varsigma}_k(m)\boldsymbol{\varsigma}^*_{k'}(m')\right\} = \boldsymbol{\Psi}(m)\delta_{k,k'}\delta_{m,m'}. \tag{21}
$$

The matrices $\boldsymbol{\Psi}$ are real from Remark 1. Additionally, it is commonplace to assume that the dynamic uncertainties appearing in Eqn. (11) are not correlated with the measurement uncertainties, i.e.,

$$
E\left\{\boldsymbol{\eta}_k(m)\boldsymbol{\varsigma}^*_{k'}(m')\right\} = \mathbf{0}. \tag{22}
$$

The extended Kalman filter (EKF) is an ad hoc modification of the KF to address nonlinear systems. For its implementation, one needs to know the Jacobian of the relevant vector fields. Since the quadratic nonlinearity in the complex domain appearing in Eqn. (19) does not satisfy the Cauchy-Riemann equations for complex differentiability, the requisite Jacobian cannot be computed directly. The solution is to separate the real and imaginary parts of the state and output equations. A brief outline of the procedure follows.

Let the real and imaginary components of any quantity be denoted by superscripts r and i, respectively. Using the definitions appearing in Eqns. (6), (7), (11), and (20), specify the following *real* vectors encompassing all azimuthal Fourier modes

$$
\breve{\boldsymbol{\alpha}}_k := \left[\{\boldsymbol{\alpha}_k(0)\}^{\mathrm{T}} \ \{\boldsymbol{\alpha}^r_k(1)\}^{\mathrm{T}} \ \cdots \ \{\boldsymbol{\alpha}^r_k(N_m)\}^{\mathrm{T}} \ \{\boldsymbol{\alpha}^i_k(1)\}^{\mathrm{T}} \ \cdots \ \{\boldsymbol{\alpha}^i_k(N_m)\}^{\mathrm{T}} \right]^{\mathrm{T}} \in \mathbb{R}^{N_n(2N_m+1)},
$$
$$
\breve{\mathbf{p}}_k := \left[\{\hat{\mathbf{p}}_k(0)\}^{\mathrm{T}} \ \{\hat{\mathbf{p}}^r_k(1)\}^{\mathrm{T}} \ \cdots \ \{\hat{\mathbf{p}}^r_k(N_m)\}^{\mathrm{T}} \ \{\hat{\mathbf{p}}^i_k(1)\}^{\mathrm{T}} \ \cdots \ \{\hat{\mathbf{p}}^i_k(N_m)\}^{\mathrm{T}} \right]^{\mathrm{T}} \in \mathbb{R}^{N_p(2N_m+1)},
$$
$$
\breve{\boldsymbol{\eta}}_k := \left[\{\boldsymbol{\eta}_k(0)\}^{\mathrm{T}} \ \{\boldsymbol{\eta}^r_k(1)\}^{\mathrm{T}} \ \cdots \ \{\boldsymbol{\eta}^r_k(N_m)\}^{\mathrm{T}} \ \{\boldsymbol{\eta}^i_k(1)\}^{\mathrm{T}} \ \cdots \ \{\boldsymbol{\eta}^i_k(N_m)\}^{\mathrm{T}} \right]^{\mathrm{T}} \in \mathbb{R}^{N_n(2N_m+1)},
$$
$$
\breve{\boldsymbol{\varsigma}}_k := \left[\{\boldsymbol{\varsigma}_k(0)\}^{\mathrm{T}} \ \{\boldsymbol{\varsigma}^r_k(1)\}^{\mathrm{T}} \ \cdots \ \{\boldsymbol{\varsigma}^r_k(N_m)\}^{\mathrm{T}} \ \{\boldsymbol{\varsigma}^i_k(1)\}^{\mathrm{T}} \ \cdots \ \{\boldsymbol{\varsigma}^i_k(N_m)\}^{\mathrm{T}} \right]^{\mathrm{T}} \in \mathbb{R}^{N_p(2N_m+1)}.
$$

Then the new set of state and output equations are

$$
\breve{\boldsymbol{\alpha}}_{k+1} = \breve{\mathbf{F}}\breve{\boldsymbol{\alpha}}_k + \breve{\boldsymbol{\eta}}_k, \tag{23a}
$$
$$
\breve{\mathbf{p}}_k = \breve{\mathbf{h}}\left(\breve{\boldsymbol{\alpha}}_k\right) + \breve{\boldsymbol{\varsigma}}_k. \tag{23b}
$$

The new state transition matrix is a block-diagonal concatenation of the matrices appearing in Eqn. (11):

$$
\breve{\mathbf{F}} := \mathrm{diag}\left(\left[\ \mathbf{F}(0) \quad \mathbf{F}(1) \quad \cdots \quad \mathbf{F}(N_m) \quad \mathbf{F}(1) \quad \cdots \quad \mathbf{F}(N_m) \ \right]\right).
$$

The real quadratic nonlinearity in the output equation is denoted by the operator $\breve{\mathbf{h}} : \mathbb{R}^{N_n(2N_m+1)} \to \mathbb{R}^{N_p(2N_m+1)}$. It can be expressed in terms of the parameters appearing in Eqn. (19); the details are omitted

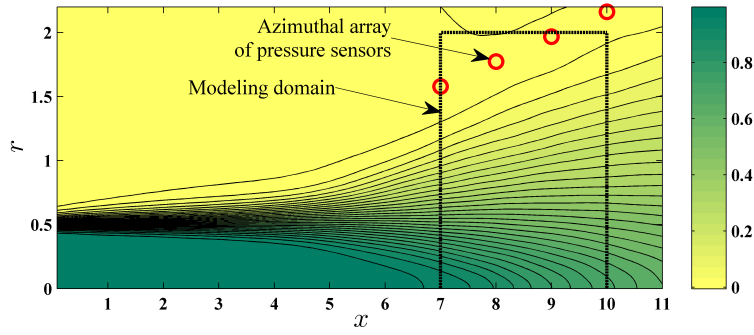American Institute of Aeronautics and Astronautics

Figure 2. Meridional half-slice of jet shear layer showing contour plot of mean axial velocity from the DNS database. The cross-section of the cylindrical modeling domain is indicated. Additionally, the locations of the ring arrays of pressure sensors are depicted.

due to space constraints. In its new form, the Jacobian can be obtained in a straightforward manner; using the formalism from Section III.B.1, the specific notation is

$$\breve{\mathbf{H}}_k^{\mathrm{T}} := \left.\frac{\partial \breve{\mathbf{h}}}{\partial \breve{\boldsymbol{\alpha}}}\right|_{\breve{\boldsymbol{\alpha}} = \tilde{\boldsymbol{\alpha}}_{k/k-1}}.$$

Recall that the covariances of the complex uncertainty sequences are real, and they are uncorrelated across azimuthal modes. Then it can be shown that the real and imaginary parts of the uncertainty sequences each contribute a half of the total covariance. Thus new zero-mean real uncertainty sequences satisfy the relations

$$E\left\{\breve{\boldsymbol{\eta}}_k\breve{\boldsymbol{\eta}}_{k'}^*\right\} = \breve{\boldsymbol{\Upsilon}}\delta_{k,k'} = \mathrm{diag}\left(\begin{bmatrix} \boldsymbol{\Upsilon}(0) & 0.5\boldsymbol{\Upsilon}(1) & \cdots & 0.5\boldsymbol{\Upsilon}(N_m) & 0.5\boldsymbol{\Upsilon}(1) & \cdots & 0.5\boldsymbol{\Upsilon}(N_m) \end{bmatrix}\right)\delta_{k,k'},$$

$$E\left\{\breve{\boldsymbol{\varsigma}}_k\breve{\boldsymbol{\varsigma}}_{k'}^*\right\} = \breve{\boldsymbol{\Psi}}\delta_{k,k'} = \mathrm{diag}\left(\begin{bmatrix} \boldsymbol{\Psi}(0) & 0.5\boldsymbol{\Psi}(1) & \cdots & 0.5\boldsymbol{\Psi}(N_m) & 0.5\boldsymbol{\Psi}(1) & \cdots & 0.5\boldsymbol{\Psi}(N_m) \end{bmatrix}\right)\delta_{k,k'},$$

$$E\left\{\breve{\boldsymbol{\eta}}_k\breve{\boldsymbol{\varsigma}}_{k'}^*\right\} = \mathbf{0}.$$

With this model setup, the equations for the extended Kalman filter follow directly from Ref. 39. Extending the notation from Section III.B.1, one obtains

$$\breve{\mathbf{K}}_k = \breve{\mathbf{F}}\breve{\boldsymbol{\Gamma}}_{k/k-1}\breve{\mathbf{H}}_k\left(\breve{\mathbf{H}}_k^{\mathrm{T}}\breve{\boldsymbol{\Gamma}}_{k/k-1}\breve{\mathbf{H}}_k + \breve{\boldsymbol{\Psi}}\right)^{-1}, \tag{24a}$$

$$\tilde{\boldsymbol{\alpha}}_{k+1/k} = \breve{\mathbf{F}}\tilde{\boldsymbol{\alpha}}_{k/k-1} + \breve{\mathbf{K}}_k\left(\breve{\mathbf{p}}_k - \breve{\mathbf{h}}\left(\tilde{\boldsymbol{\alpha}}_{k/k-1}\right)\right), \tag{24b}$$

$$\breve{\boldsymbol{\Gamma}}_{k+1/k} = \left(\breve{\mathbf{F}} - \breve{\mathbf{K}}_k\breve{\mathbf{H}}_k^{\mathrm{T}}\right)\breve{\boldsymbol{\Gamma}}_{k/k-1}\left(\breve{\mathbf{F}} - \breve{\mathbf{K}}_k\breve{\mathbf{H}}_k^{\mathrm{T}}\right)^{\mathrm{T}} + \breve{\boldsymbol{\Upsilon}} + \breve{\mathbf{K}}_k\breve{\boldsymbol{\Psi}}\breve{\mathbf{K}}_k^{\mathrm{T}}, \tag{24c}$$

$$\tilde{\boldsymbol{\alpha}}_{0/-1} = \mathbf{0}, \tag{24d}$$

$$\breve{\boldsymbol{\Gamma}}_{0/-1} = \mathrm{diag}\left(\Lambda^{(1)}(0) \quad \cdots \quad \Lambda^{(N_n)}(0) \; 0.5\Lambda^{(1)}(1) \quad \cdots \quad 0.5\Lambda^{(N_n)}(1) \quad \cdots \quad 0.5\Lambda^{(1)}(N_m) \quad \cdots \quad 0.5\Lambda^{(N_n)}(N_m)\right.$$

$$\left. 0.5\Lambda^{(1)}(1) \quad \cdots \quad 0.5\Lambda^{(N_n)}(1) \quad \cdots \quad 0.5\Lambda^{(1)}(N_m) \quad \cdots \quad 0.5\Lambda^{(N_n)}(N_m)\right). \tag{24e}$$

The form of the RHS for the last equation follows from the argument made for obtaining the uncertainty covariances above. One notes that the EKF relations are no longer decoupled for the various azimuthal modes. Moreover, the linearized dynamics have become time-varying owing to the time-dependence of $\breve{\mathbf{H}}$.

IV.   Results

The details of the direct numerical simulation database are available in Ref. 8; here only the the most pertinent aspects are highlighted. The computational data is saved at 2316 consecutive time instants with uniform separation of 0.071 (in t^+ coordinates). A contour plot of the mean axial velocity is shown in Figure 2. A POD-GP reduced-order model of the indicated domain, covering the end of the potential core, has been previously developed by the authors.[7] The ROM has 30-states, viz. POD modes from 1 through 5 and azimuthal Fourier modes from 0 to 5; thus $N_n = N_m = 5$.

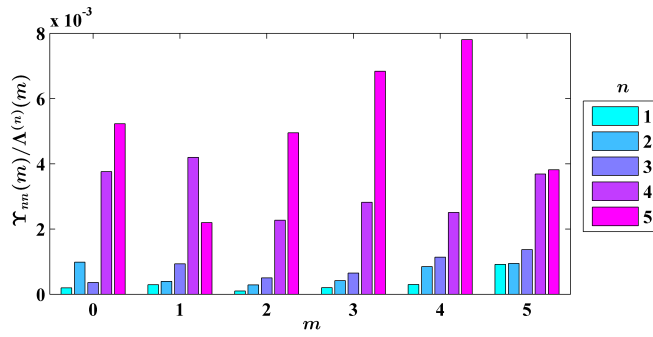American Institute of Aeronautics and Astronautics

Figure 3. Diagonal terms of state uncertainty covariance normalized by the respective POD eigenvalues.

For practical implementation, the pressure sensors should be placed upstream of the modeling domain, closer to the nozzle exit plane. This would introduce significant lags between the model state dynamics and the measured pressure. In future, the strategies developed here will be extended to the configuration of upstream pressure sensing. However, to avoid the attendant complications, this preliminary attempt at real-time state estimation proceeded by assuming that the pressure measurements are available at some or all of the azimuthal ring arrays of sensors shown in Figure 2 (refer also to Figure 1). The four rings are on the surface of a virtual cone with half-angle 11° that parallels the outer edge of the shear layer; they are uniformly spaced between $x = 7$ and 10, with the radius of the most upstream ring being $r = 1.58$. The cylindrical computational grid has 80 uniformly spaced azimuthal grid-points; virtual sensors were placed at each of these points.

The set of snapshots was halved into two mutually exclusive random sets. The various estimation models discussed in Section III were built using the statistics educed from the first set (the *training set*). The fidelity of estimation was then tested for each of the strategies using the second set (the *validation set*). This division of training and validation datasets is ideal for stochastic estimation. However, the IIR filters require the entire time-history of the output, so that the distinction is not as well-defined. The IIR filter models were developed solely from the training set, and are simulated using the time-resolved pressure from the entire database. Finally, the samples corresponding to the validation dataset were selected to evaluate the performance.

The family of state transition matrices $\mathbf{F}$ have been determined in Ref. 7. One of the advantages of having the DNS database is that the modeling uncertainty sequences $\boldsymbol{\eta}$ are directly available, so that their covariances $\boldsymbol{\Upsilon}$ can also be ascertained (see Eqn. (12) for the definition). The diagonal terms of these covariance matrices are shown in Figure 3; the off-diagonal terms were found to be substantially smaller by comparison.

The next focus is on the linear output relation for the Kalman filter appearing in Eqn. (13). Recall from Eqn. (16) that the coefficients $\mathbf{L}_{KF}$ are to be determined by an application of LSE to the empirical data. This warrants a study of the following set of normalized cross-correlation coefficients

$$\zeta_{\alpha p}^{(n)}(s, m) := \frac{E\left\{\alpha_k^{(n)}(m)\hat{p}_k^*(s, m)\right\}}{\sqrt{\Lambda^{(n)}(m)E\left\{|\hat{p}_k(s, m)|^2\right\}}}, \quad (s, m, n) \in [1, N_p] \times [0, N_m] \times [1, N_n]. \qquad (25)$$

Here, Eqn. (4b) is invoked to make the substitution $\Lambda^{(n)}(m) = E\left\{\left|\alpha_k^{(n)}(m)\right|^2\right\}$. Note that the cross-correlation coefficients are real following Remark 1. The above statistics are also relevant to the direct LSE model (see Eqns. (8) and (9)), which is a dual of the linear KF output relation.

The convergence of the above statistics was assessed for the DNS database. In particular, the correlation coefficients were evaluated from the training dataset, as well as from the full database, and the differences were found to be insignificant. In Figure 4, the absolute values of $\zeta_{\alpha p}$ are plotted. This should be analyzed from two perspectives. In determining the accuracy of the KF output relation for pressure at a particular axial location and azimuthal mode (i.e., fixed s and m), one is seeking high correlation levels for *any* POD mode n. From this perspective, it is easy to determine that the ring array at $x_s = 8$ is optimal. However, the ultimate goal is to *observe* the POD modal coefficients from the pressure. For observability, one is seeking
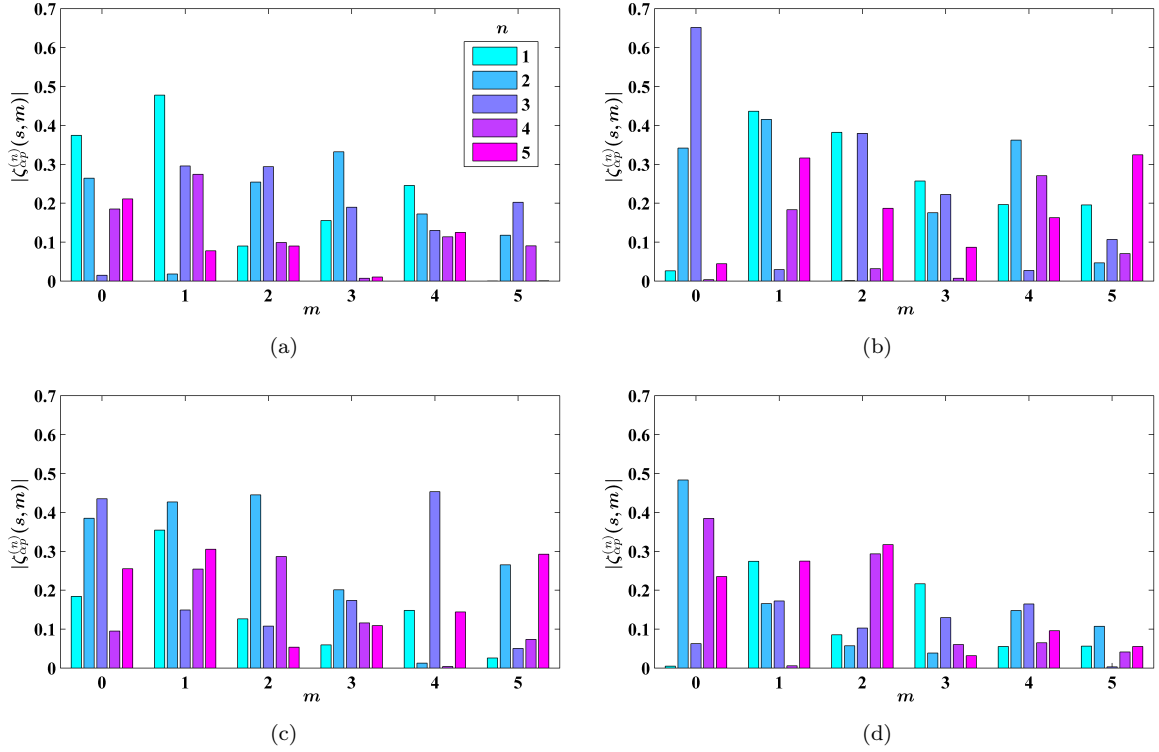
American Institute of Aeronautics and Astronautics

Figure 4. Second-order pressure-POD mode correlations for sensor ring array at axial locations of (a) 7, (b) 8, (c) 9, and (d) 10.

high correlation levels for *all* POD modes. From this perspective, one finds that no single axial location of pressure sensing can be used exclusively for direct LSE, and one may need measurements at multiple axial locations. Since the linear KF uses an approximate knowledge of the dynamic coupling of the different POD modes in addition to the static output relation, it may be expected to perform better.

A similar study can be made of the third order moments involved in the QSE that determines the quadratic output equation for the extended Kalman filter in Eqn. (19). The relevant set of normalized correlation coefficients is

$$
\zeta_{\alpha\alpha p}^{(nn')}(s,m,m') := \frac{E\left\{\alpha_k^{(n)}(m')\alpha_k^{(n')}(m-m')\hat{p}_k^*(s,m)\right\}}{\sqrt{\Lambda^{(n)}(m')\Lambda^{(n')}(m-m')E\left\{|\hat{p}_k(s,m)|^2\right\}}},
$$

$$
(s,m,n,n') \in [1,N_p] \times [0,N_m] \times [1,N_n] \times [1,N_n], \ m' \in [m-N_m,N_m]. \tag{26}
$$

These statistics are real following Remark 1. In Figure 5, the absolute values of $\zeta_{\alpha\alpha p}$ are depicted for some representative combinations. These third order moments are not insignificant compared to the second order moments in Figure 4. Thus, a quadratic model can be expected to be significantly more accurate than a linear one.

The accuracies of the linear and quadratic output models can be assessed from their respective output uncertainty covariance matrices $\mathbf{\Xi}$ and $\mathbf{\Psi}$; see Eqns. (14) and (21). The diagonal elements of these matrices (indicated by the repeated subscripts) are shown in Figure 6, normalized by the variances of the respective pressure signals. The off-diagonal elements were generally smaller. For converged statistics, use of the LSE in determining the relevant parameter vectors $\mathbf{L}_{KF}$, along with the orthogonality of the POD modal coefficients seen in Eqn. (4b), leads to the following simplification

$$
\frac{\Xi_{ss}(m)}{E\left\{|\hat{p}_k(s,m)|^2\right\}} = 1 - \sum_{n=1}^{N_n}\left|\zeta_{\alpha p}^{(n)}(s,m)\right|^2.
$$

Referring to Figure 6, several remarks can be made:

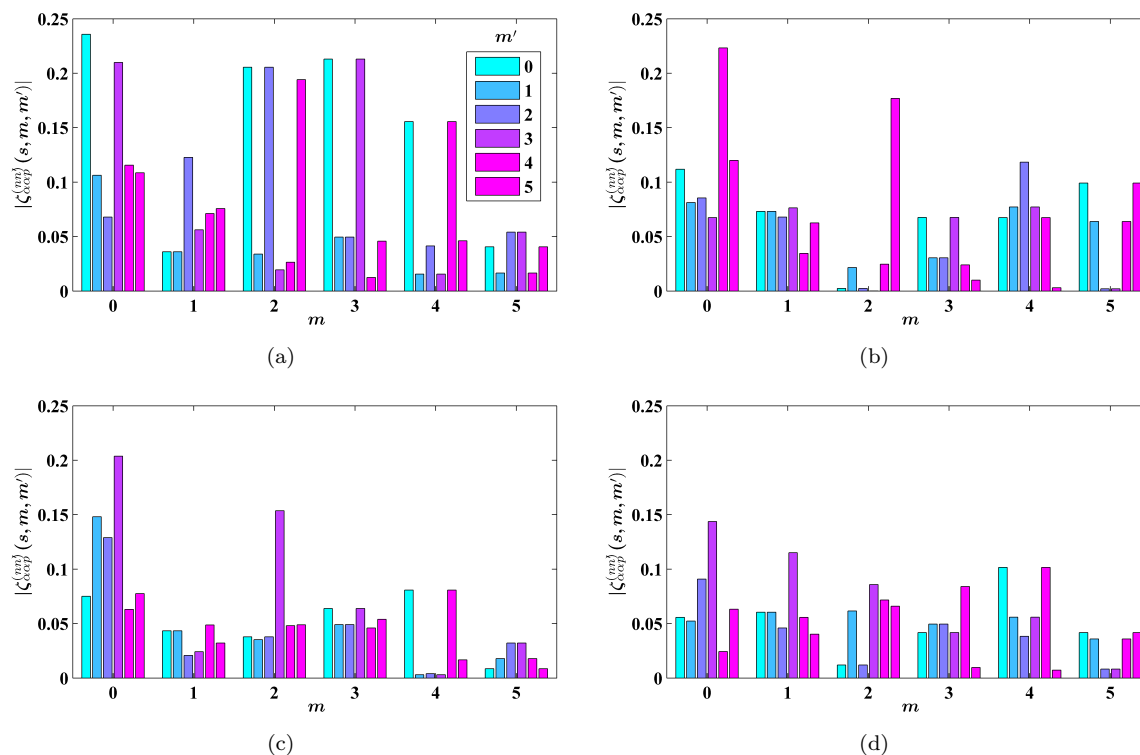American Institute of Aeronautics and Astronautics

Figure 5. Selected third-order pressure-POD mode correlations for the ring array located at $x_s = 8$, and $n = n'$. The POD modes depicted are (a) 1, (b) 2, (c) 3, and (d) 4.

- Since the filter models should be built exclusively from the training set, both the fit parameters as well as the covariances were evaluated on the same training set. However, similar values of covariances were also obtained when the entire database was used for validation, again attesting to the convergence of relevant statistics.

- For the specified 30-state model, the linear output equation had 5 parameters (corresponding to the 5 POD modes) to fit the empirical data for each azimuthal mode m and each ring array location indexed by s. On the other hand, the quadratic output equation had anywhere from 85 (for $m = 5$) to 145 (for $m = 0$) parameters to fit the same empirical data for each $m - s$ combination (see Appendix A).

- The substantial increase of accuracy in going from a linear to a quadratic model indicates that third order statistical moments are indeed significant.

- As expected, use of the ring arrays in the middle of the axial zone considered demonstrate greater accuracy compared to the rings at the upstream and downstream extremes.

Two different configurations of pressure sensor ring arrays are evaluated. For practical implementation, a single ring array is obviously preferable. Thus, for reasons discussed above, the "solo" performance of the ring array at $x_s = 8$ is assessed. This configuration is denoted by $\mathcal{X}_p = \{8\}$. At the other extreme, all four ring arrays were also considered in tandem to assess the limits of the estimation strategies presented herein. This configuration is $\mathcal{X}_p = \{7, 8, 9, 10\}$.

The state transition matrices $\mathbf{F}(m)$ for the educed ROM in Eqn. (11) were found to be unstable. However, the detectability and stabilizability criteria for the linear KF mentioned in Section III.B.1 were satisfied in both sensor configurations discussed above; this guarantees filter stability. The trajectories of selected filter gains for $\mathcal{X}_p = \{8\}$ are shown in Figure 7. For the KF, the gains reach the stationary values predicted by Eqns. (18) and (17a) within 25 flow time steps. Since the EKF model is time-varying, its gains never reach steady-state. However, the gains are seen to be within tight bounds in this simulation after about 20 flow time steps.

The preceding discussion has established the characteristics of the models for KF and EKF. Owing to their duality, the characteristics of the LSE and QSE models expressed in Eqns. (8) and (10) have also been
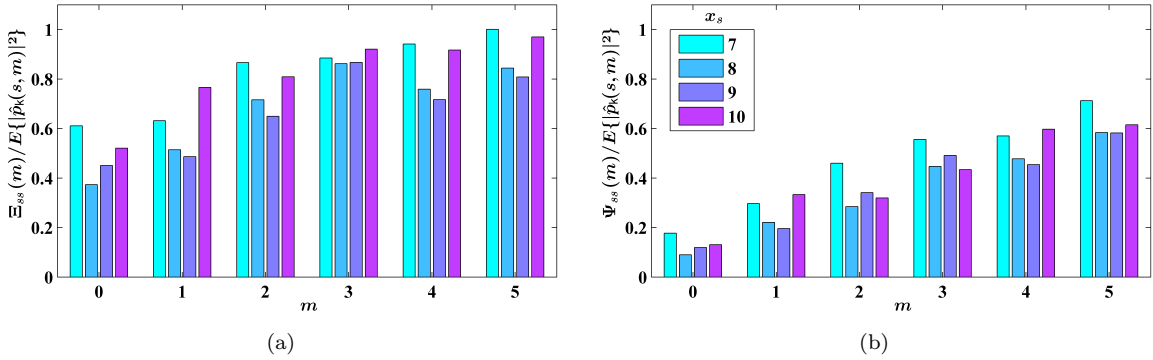
American Institute of Aeronautics and Astronautics

Figure 6. Diagonal terms of output uncertainty covariance matrices normalized by the respective pressure variances for (a) linear output equation, and (b) quadratic output equation.
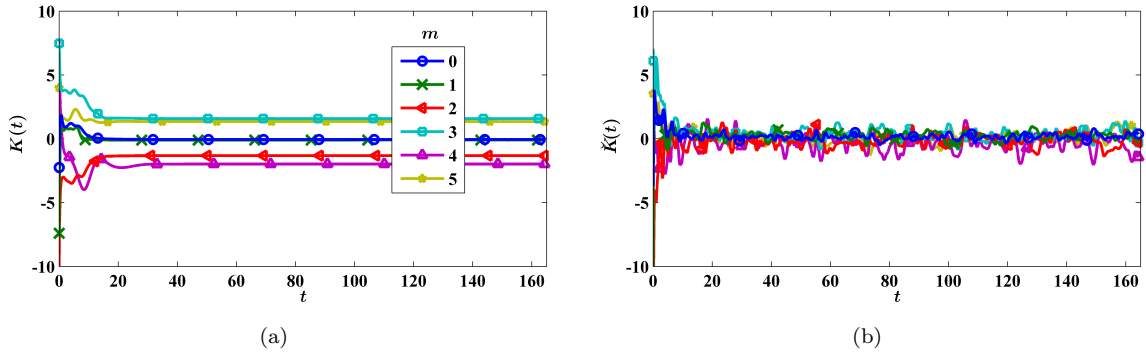

Figure 7. Trajectories of selected gains in the $\mathcal{X}_p = \{8\}$ configuration. (a) KF gains from $\hat{p}(x_s = 8, m)$ to $\alpha^{(1)}(m)$. (b) EKF gains from $\hat{p}^r(x_s = 8, m)$ to $\alpha^{(1)r}(m)$. The discrete time step has been scaled to the flow time step t^+.

described in the process. To gain an understanding of the behavior of these estimators, the trajectories of two states estimated in the $\mathcal{X}_p = \{8\}$ configuration are shown in Figure 8. Based on the results presented in Figure 8, the following remarks are in order.

- The KF and EKF demonstrate similar performance, in spite of the order-of-magnitude increase in computational complexity in the latter.

- There are substantial initial inaccuracies in the KF and EKF for $m = 0$, although both demonstrate much improvement in fidelity at later times. On the other hand, for $m = 1$, they perform quite satisfactorily from the beginning.

- The LSE essentially gives a null result for $m = 0$, but its performance is much improved for $m = 1$. This could have been predicted from the low value of $\zeta_{\alpha p}^{(1)}(x_s = 8, 0)$ seen in Figure 4. This makes the superior performance of the KF all the more remarkable in this case. The improved fidelity of LSE for the $m = 1$ case could also have been predicted from the higher value of $\zeta_{\alpha p}^{(1)}(x_s = 8, 1)$.

- Compared to LSE, use of QSE significantly improves the estimation performance in the instance of $m = 0$, with an attendant increase in computational cost. However, in the $m = 1$ case, QSE does not demonstrate any obvious improvement over LSE.

While the above analysis gave some insight, they are somewhat anecdotal since only two states were considered. To quantitatively compare the overall performance of the various state estimators, the following
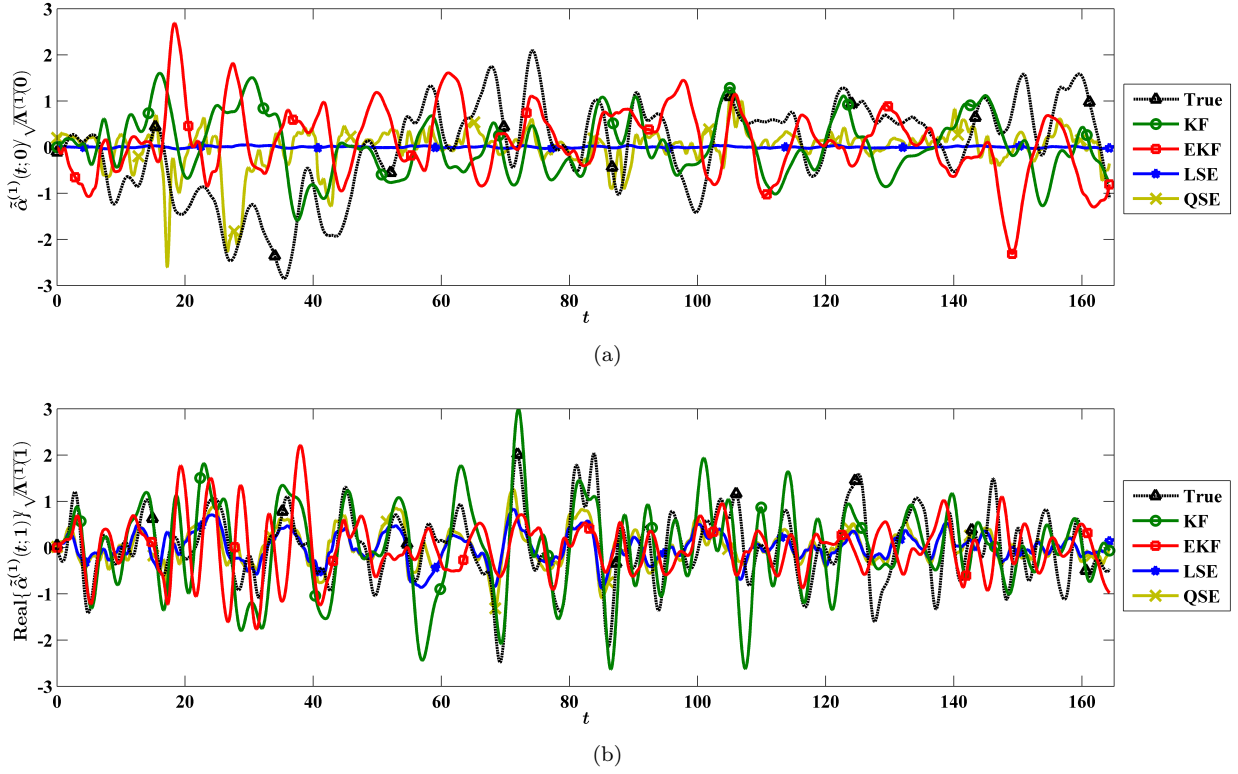
American Institute of Aeronautics and Astronautics

Figure 8. Estimated trajectories of selected states with various strategies in the $\mathcal{X}_p = \{8\}$ configuration. The discrete time step has been scaled to the flow time step t^+.

family of metrics are established

$$
\hat{e}_\alpha^{(n)}(m) := \frac{E\left\{\left|\tilde{\alpha}_{k/k-1}^{(n)}(m) - \alpha_k^{(n)}(m)\right|^2\right\}}{\sqrt{E\left\{\left|\alpha_k^{(n)}(m)\right|^2\right\} E\left\{\left|\tilde{\alpha}_{k/k-1}^{(n)}(m)\right|^2\right\}}}.
\tag{27}
$$

The notation is aligned with the Kalman filter, but simply substituting $\tilde{\alpha}_{k/k-1}$ with $\tilde{\alpha}_k$ makes it suitable for assessing the performance of the stochastic estimators too. Note that $0 \leq \hat{e}_\alpha < \infty$. A value close to 0 indicates higher fidelity. The metric will have a moderate value if the instantaneous estimation is not accurate, but the variance of the state α is well-replicated by the estimate $\tilde{\alpha}$. On the other hand, $\hat{e}_\alpha$ will become large whenever the variance of the estimate is significantly disparate from that of the state. The latter aspect is particularly useful for detecting the poor performance of LSE as seen in Figure 8(a).

The estimation error metric is evaluated using the validation dataset for the two sensing configurations and the four estimation techniques discussed so far. The results are presented in Figure 9. Several conclusions can be drawn from this figure.

- In the single ring configuration, the KF strategy demonstrates the least overall estimation error. For the $m = 4$ case, its performance is poorer than the EKF. Both the single-time stochastic estimators perform poorly. LSE alone is of course not a viable option for state-estimation, as succinctly demonstrated by the need for the logarithmic ordinate scale.

- When all four sensor ring arrays are used, the QSE represents the best strategy. The LSE demonstrates a marked improvement over its performance in $\mathcal{X}_p = \{8\}$ case. In fact, the KF and EKF have the least significant improvement compared to their respective performances in the single ring configuration. The KF again outperforms the EKF, and both show better accuracy compared to LSE. Given the experimental limitations, one would obviously prefer KF and EKF over SE.
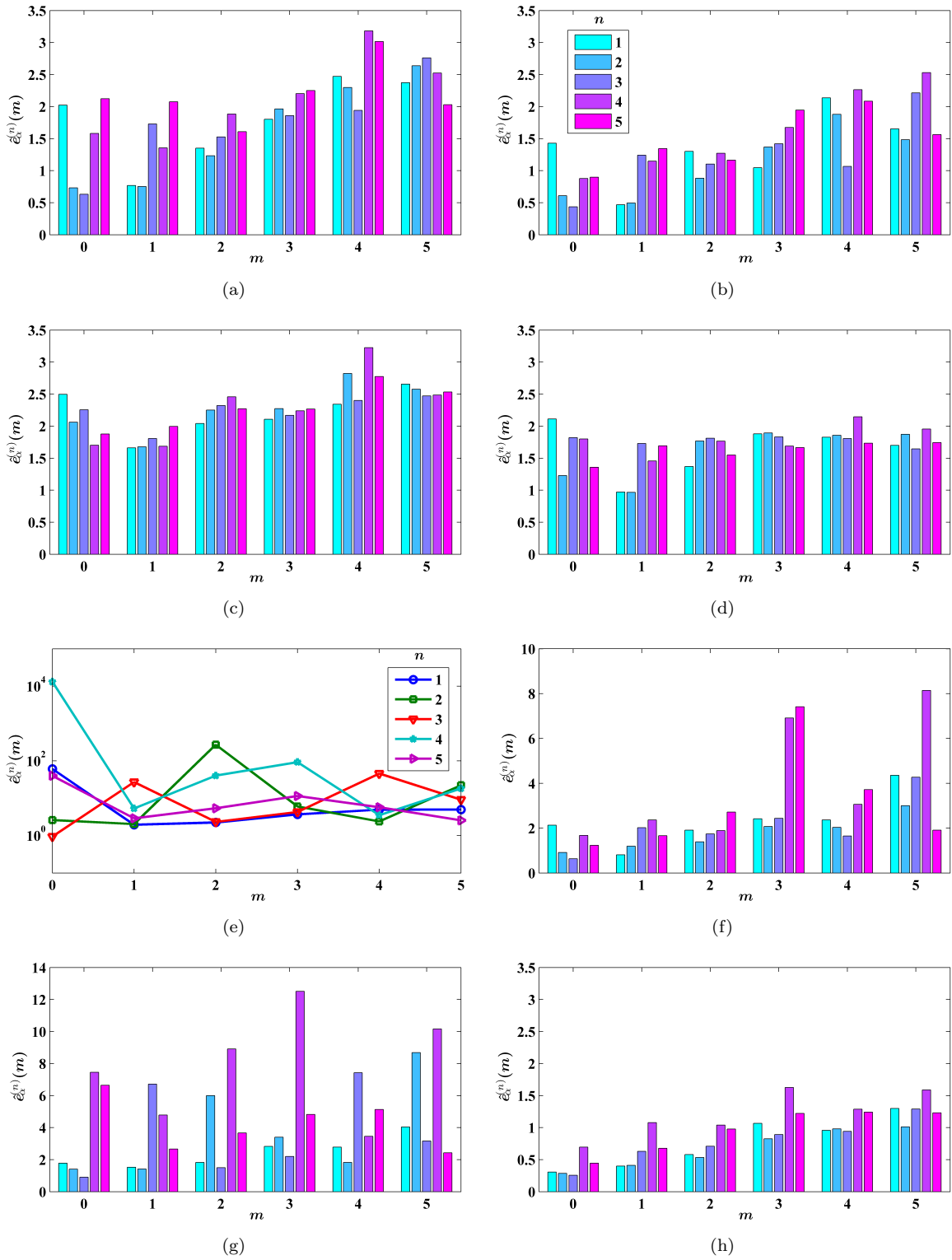
Figure 9. The POD modal coefficient estimation error metrics using (a) & (b) Linear Kalman filter, (c) & (d) Extended Kalman filter, (e) & (f) LSE, and (g) & (h) QSE. In (a), (c), (e), & (g) $\mathcal{X}_p = \{8\}$, and in (b), (d), (f), & (h) $\mathcal{X}_p = \{7, 8, 9, 10\}$. Note that the ordinate scales are different.

American Institute of Aeronautics and Astronautics

- In both configurations, QSE represents a very significant improvement on the LSE strategy. This attests to the nonlinearity of the pressure-velocity interaction in the jet near-field.

- The EKF generally demonstrates a performance degradation over the much simpler KF. This shows that the increased complexity of the EKF makes it difficult to tune. A different choice of uncertainty covariance parametrization may have improved the estimation, but the correct value to adopt is not obvious.

The steady-state Kalman gains given by Eqns. (18) and (17a) can be computed a priori, and used in the linear time-invariant filter (LTIF). Compared to the time-varying KF, the discrepancy in performance is not expected to persist for long beyond 25 flow time steps from initiation (see Figure 7(a), and the discussion thereof). As mentioned before, the LTIF is similar in complexity to the single-time LSE model, and thus it is an attractive estimation strategy provided that its performance is comparable to the KF *within* the transient period. This was indeed verified to be true for both pressure sensor configurations considered; the results are not shown. The very significant accuracy improvement in going from LSE or QSE to KF has been remarked previously.

V. Conclusions

In real-time state estimation for feedback flow control, as in any engineering field, an essential dilemma is between simplicity and performance. Single-time and multi-time linear and quadratic stochastic estimators have long been the preferred strategy due to their simplicity. At heart, these are essentially curve-fitting techniques that do not exploit any knowledge of the flow dynamics, if available. A major shortcoming of such estimators is that they pass measurement noise unfiltered to the state estimate. Moreover, some flow states may not have a direct static relation with the measured output, but may only be observable indirectly through coupled dynamics.

In certain flow systems, a time-invariant linearized model of the dynamics may be at hand, along with an approximate measure of the modeling and measurement uncertainties. In this case, a time-invariant infinite-memory filter may yield an improved estimation with minimal increase in runtime complexity over the linear stochastic estimator. The two shortcomings of stochastic estimators mentioned above may both be mitigated by this technique. The infinite memory of the filter is the result of a recursive update strategy for the state estimate. A time-invariant filter may suffer from large transients in state estimation error, which may be addressed by a linear time-varying Kalman filter. The major increase in complexity in the latter is due to the necessity of inverting a matrix of the size of the measurement vector at every time step.

If a nonlinear state and/or output equation is available, then an ad hoc extension of the linear Kalman filter may be implemented. Such an extended Kalman filter is necessarily sub-optimal; moreover the increasing complexity may even lead to a degradation of fidelity if the filter is not tuned exactly. The large amount of computations necessary at every time step may overwhelm hardware capabilities. Finally, unlike the linear filter, closed-form stability and performance analyses are typically not possible for the nonlinear filter.

In this article, all the above estimation strategies were implemented and assessed using a well-established direct numerical simulation database of a high-speed axisymmetric jet. The authors have recently developed a reduced-order model of the shear layer of this jet using Proper Orthogonal Decomposition and Galerkin Projection. To cover the important region of the end of the potential core, the axial extent of the modeling domain was between 7 and 10 jet diameters downstream of the nozzle exit. The pressure in the irrotational near-field has long been surmised to be an ideal measurement for estimating the state of the shear layer in real-time. For practical implementation, the pressure sensors should be close to the nozzle exit, upstream of the modeling domain. However, to avoid modeling complications arising out of the delays involved thereof, this preliminary assessment investigated the following two sensor configurations. The first one considered using a single azimuthal ring array of sensors, and the optimal location for this was found to be at 8 jet diameters downstream. To explore the limits of the estimation strategies, the other configuration had four such arrays distributed uniformly over the axial domain of the model, outside the shear layer.

For the single ring configuration, single-time linear stochastic estimation was found to be quite unsuitable, since some states of the model are not linearly related to this pressure signal. The quadratic stochastic estimation yielded significant improvements in accuracy, bearing testimony to the essential nonlinearity in the pressure-velocity coupling. The linear time-invariant filter and linear time-varying Kalman filters were

demonstrated to have similar fidelity, and both out-performed the quadratic stochastic estimator by large margins. This shows the distinct benefit to be accrued in moving to a dynamic model-based estimation strategy. It is to be emphasized that the linear time-invariant filter is similar in complexity to the linear stochastic estimator, and considerably less resource-intensive than the quadratic stochastic estimator. The extended Kalman filter is significantly more complicated, but it actually under-performed the linear filters, possibly owing to inexact tuning.

When all four sensor ring arrays were used, the linear stochastic estimator showed a marked improvement; however, it still performed worse than the other strategies. The model-based filters showed meagre gains in fidelity. The single-time quadratic stochastic estimator demonstrated the best performance in this configuration. This reflects the improved curve-fitting that is possible when a large number of fit-parameters are available, and higher order statistical moments are not insignificant. One of the contributions of this article is the exposition of the multi-point quadratic stochastic estimator algorithm in the Fourier domain.

The work presented herein may be extended in several important ways. At an earlier stage, the authors have demonstrated the improvement in offline estimation performance accrued by adding an axially extended linear array of pressure sensors to an azimuthal ring array. Such a sensor configuration is much more feasible than requiring multiple ring arrays of sensors. This configuration will be investigated for efficacy in a real-time estimation application involving a model-based filter. To bring the strategies developed herein to bear on a practical implementation, the sensor ring array must also be moved upstream. This would make the estimation more reliant on the dynamic model, so that one may have to resort to the more accurate quadratic reduced-order model developed originally in Ref. 7. Finally, the estimation strategies developed here address a model of the unforced jet. The applicability of these strategies in the case of a forced jet will be investigated in our future work.

Acknowledgments

Appendix A.   Implementing QSE in a Fourier Domain

Consider a flow with a homogenous direction. Suppose that a family of N distinct fields are simultaneously measured over respective grids that are fine enough in the homogenous direction to resolve all Fourier modes in the range $m \in [-M, M]$. The measured fields will be denoted by $\hat{z}_k(s, m)$, where k refers to the sample index for the sampled-data system, s is the index running from 1 to N that identifies a particular field in the family, and m refers to the Fourier mode. Consider another field $\hat{w}_k(m)$ that is to be estimated from the measured fields in the same Fourier domain. All fields are assumed to be zero-mean. The extension to estimation in the continuous time domain is trivial.

The most general multi-point single-time quadratic estimator of $\hat{w}_k$ is

$$\tilde{\hat{w}}_k(m) = \delta_{m,0} c^*_{QSE} + \sum_{s=1}^{N} l^*_{QSE}(s, m) \hat{z}_k(s, m)$$

$$+ \sum_{m'=m-M}^{M} \sum_{s,s'=1}^{N} q^*_{QSE}(s', s, m', m - m') \hat{z}_k(s, m') \hat{z}_k(s', m - m'), \qquad m \in [0, M].$$

Here, Remark 2 is invoked to argue that the particular products of Fourier modes considered above are the only ones that have non-vanishing correlations with $\hat{w}_k(m)$. The expectations of all linear terms are zero. The expectations of all quadratic terms are also zero, except for $E\{\hat{z}_k(s, 0)\hat{z}_k(s', 0)\}$; the constant term ensures that $E\{\tilde{\hat{w}}_k(m)\} = 0$, for all m. The complex conjugations, and the related inversion in the order of s and s' in q_{QSE}, are for ease of matrix manipulation.

For consistency of the above model, the quadratic estimation parameters necessarily satisfy the symmetry

American Institute of Aeronautics and Astronautics

condition $q_{QSE}(s, s', m', m'') = q_{QSE}(s', s, m'', m')$. This results in a redundancy, which is removed thus

$$\tilde{w}_k(m) = \delta_{m,0} c_{QSE}^* + \sum_{s=1}^{N} l_{QSE}^*(s, m) \hat{z}_k(s, m) + \sum_{m'=m-M}^{\lfloor m/2 \rfloor} \sum_{s=1}^{N} \overrightarrow{q}_{QSE}^*(s, s, m', m - m') \hat{z}_k(s, m') \hat{z}_k(s, m - m')$$

$$+ \sum_{m'=m-M}^{M} \sum_{s=1}^{N-1} \sum_{s'=s+1}^{N} \overrightarrow{q}_{QSE}^*(s', s, m', m - m') \hat{z}_k(s, m') \hat{z}_k(s', m - m'), \quad m \in [0, M].$$

Here $\lfloor \cdot \rfloor$ indicates the `floor` function. For later reference, the `ceiling` function is $\lceil \cdot \rceil$. The new quadratic estimation parameters $\overrightarrow{q}_{QSE}$ form a family of lower triangular matrices for any fixed Fourier mode pair. The entries of $\overrightarrow{q}_{QSE}$ that do not appear in the above expression are understood to be identically zero. The original quadratic parameters can be retrieved as

$$q_{QSE}(s, s', m', m - m') = \begin{cases} \overrightarrow{q}_{QSE}(s, s', m', m - m'), & \text{if } m \text{ is even}, s = s', \text{ AND } m' = m/2, \\ \{\overrightarrow{q}_{QSE}(s, s', m', m - m') + \overrightarrow{q}_{QSE}(s', s, m - m', m')\} / 2, & \text{otherwise.} \end{cases}$$

The implementation proceeds by defining the following regressor for estimating $\hat{w}_k(m)$:

$$\overleftarrow{\hat{\mathbf{z}}}_k(m) := \begin{bmatrix} \hat{z}_k(1, m), & \cdots, & \hat{z}_k(N, m), \end{bmatrix}$$
$$\hat{z}_k(1, m - M) \hat{z}_k(1, M), \cdots, \hat{z}_k(1, \lfloor m/2 \rfloor) \hat{z}_k(1, \lceil m/2 \rceil),$$
$$\cdots, \hat{z}_k(N, m - M) \hat{z}_k(N, M), \cdots, \hat{z}_k(N, \lfloor m/2 \rfloor) \hat{z}_k(N, \lceil m/2 \rceil),$$
$$\hat{z}_k(1, m - M) \hat{z}_k(2, M), \cdots, \hat{z}_k(1, M) \hat{z}_k(2, m - M),$$
$$\cdots, \hat{z}_k(1, m - M) \hat{z}_k(N, M), \cdots, \hat{z}_k(1, M) \hat{z}_k(N, m - M),$$
$$\hat{z}_k(2, m - M) \hat{z}_k(3, M), \cdots, \hat{z}_k(2, M) \hat{z}_k(3, m - M),$$
$$\cdots, \hat{z}_k(2, m - M) \hat{z}_k(N, M), \cdots, \hat{z}_k(2, M) \hat{z}_k(N, m - M),$$
$$\cdots, \hat{z}_k(N - 1, m - M) \hat{z}_k(N, M), \cdots, \hat{z}_k(N - 1, M) \hat{z}_k(N, m - M) \big]^{\mathrm{T}}, \quad m \in [0, M],$$

$$\overrightarrow{\hat{\mathbf{z}}}_k(m) := \begin{cases} \left[1 \quad \left\{ \overleftarrow{\hat{\mathbf{z}}}_k(0) \right\}^{\mathrm{T}} \right]^{\mathrm{T}}, & \text{if } m = 0, \\ \overleftarrow{\hat{\mathbf{z}}}_k(m), & \text{if } m \in [1, M]. \end{cases}$$

The corresponding parameter vector is formed by collecting the matching terms from the estimator model

$$\overleftarrow{\mathcal{Q}}_{QSE}(m) := \begin{bmatrix} l_{QSE}(1, m), & \cdots, & l_{QSE}(N, m), \end{bmatrix}$$
$$\overrightarrow{q}_{QSE}(1, 1, m - M, M), \cdots, \overrightarrow{q}_{QSE}(1, 1, \lfloor m/2 \rfloor, \lceil m/2 \rceil),$$
$$\cdots, \overrightarrow{q}_{QSE}(N, N, m - M, M), \cdots, \overrightarrow{q}_{QSE}(N, N, \lfloor m/2 \rfloor, \lceil m/2 \rceil),$$
$$\overrightarrow{q}_{QSE}(2, 1, m - M, M), \cdots, \overrightarrow{q}_{QSE}(2, 1, M, m - M),$$
$$\cdots, \overrightarrow{q}_{QSE}(N, 1, m - M, M), \cdots, \overrightarrow{q}_{QSE}(N, 1, M, m - M),$$
$$\overrightarrow{q}_{QSE}(3, 2, m - M, M), \cdots, \overrightarrow{q}_{QSE}(3, 2, M, m - M),$$
$$\cdots, \overrightarrow{q}_{QSE}(N, 2, m - M, M), \cdots, \overrightarrow{q}_{QSE}(N, 2, M, m - M),$$
$$\cdots, \overrightarrow{q}_{QSE}(N, N - 1, m - M, M), \cdots, \overrightarrow{q}_{QSE}(N, N - 1, M, m - M) \Big]^{\mathrm{T}}, \quad m \in [0, M],$$

$$\overrightarrow{\mathcal{Q}}_{QSE}(m) := \begin{cases} \left[c_{QSE} \quad \left\{ \overleftarrow{\mathcal{Q}}_{QSE}(0) \right\}^{\mathrm{T}} \right]^{\mathrm{T}}, & \text{if } m = 0, \\ \overleftarrow{\mathcal{Q}}_{QSE}(m), & \text{if } m \in [1, M]. \end{cases}$$

With the above definitions, the QSE problem is re-written in a form that emphasizes its linearity w.r.t. the estimation parameters:

$$\tilde{w}_k(m) = \overrightarrow{\mathcal{Q}}_{QSE}^*(m) \overrightarrow{\hat{\mathbf{z}}}_k(m), \quad m \in [0, M].$$

Then, the requirement of minimizing the mean square estimation error leads to the solution

$$\overrightarrow{\boldsymbol{\mathcal{Q}}}_{QSE}(m) = E\left\{ \overrightarrow{\hat{\mathbf{z}}}_k(m) \overrightarrow{\hat{\mathbf{z}}}_k^*(m) \right\}^{-1} E\left\{ \overrightarrow{\hat{\mathbf{z}}}_k(m)\hat{w}_k^*(m) \right\}, \quad m \in [0, M].$$

As a final note, the number of estimation parameters is $N + (M - \lceil m/2 \rceil + 1)N + (2M - m + 1)N(N-1)/2$.

References

[1] Gutmark, E. J., Schadow, K. C., and Yu, K. H., "Mixing Enhancement in Supersonic Free Shear Flows," *Annu. Rev. Fluid Mech.*, Vol. 27, No. 1, 1995, pp. 375–417.

[2] Jordan, P. and Gervais, Y., "Subsonic jet aeroacoustics: associating experiment, modelling and simulation," *Experiments in Fluids*, Vol. 44, No. 1, 2008, pp. 1–21.

[3] Samimy, M., Kim, J.-H., Kastner, J., Adamovich, I., and Utkin, Y., "Active control of high-speed and high-Reynolds-number jets using plasma actuators," *Journal of Fluid Mechanics*, Vol. 578, 2007, pp. 305–330.

[4] Samimy, M., Kim, J.-H., Kastner, J., Adamovich, I., and Utkin, Y., "Active control of a Mach 0.9 jet for noise mitigation using plasma actuators," *AIAA Journal*, Vol. 45, No. 4, 2007, pp. 890–901.

[5] Utkin, Y. G., Keshav, S., Kim, J.-H., Kastner, J., Adamovich, I. V., and Samimy, M., "Development and use of localized arc filament plasma actuators for high-speed flow control," *Journal of Physics D: Applied Physics*, Vol. 40, No. 3, 2007, pp. 685–694.

[6] Sinha, A., Kim, K., Kim, J.-H., Serrani, A., and Samimy, M., "Extremizing Feedback Control of a High-Speed and High Reynolds Number Jet," *AIAA Journal*, Vol. 48, No. 2, 2010, pp. 387–399.

[7] Sinha, A., Serrani, A., and Samimy, M., "Development of Reduced-order Models for Feedback Control of Axisymmetric Jets," *48th AIAA Aerospace Sciences Meeting, AIAA Paper 2010-15*, 2010.

[8] Freund, J. B., "Noise sources in a low-Reynolds-number turbulent jet at Mach 0.9," *Journal of Fluid Mechanics*, Vol. 438, No. 1, 2001, pp. 277–305.

[9] Lumley, J. L., "The Structure of Inhomogeneous Turbulent Flows," *Atm. Turb. and Radio Wave Prop.*, edited by A. M. Yaglom and V. I. Tatarsky, Nauka, Moscow, 1967, pp. 166–178.

[10] Berkooz, G., Holmes, P., and Lumley, J., "The proper orthogonal decomposition in the analysis of turbulent flows," *Annu. Rev. Fluid Mech.*, Vol. 25, 1993, pp. 539–575.

[11] Holmes, P., Lumley, J., and Berkooz, G., *Turbulence, Coherent Structures, Dynamical Systems and Symmetry*, Cambridge University Press, 1996.

[12] Arndt, R. E. A., Long, D. F., and Glauser, M. N., "The proper orthogonal decomposition of pressure fluctuations surrounding a turbulent jet," *Journal of Fluid Mechanics*, Vol. 340, No. 1, 1997, pp. 1–33.

[13] Picard, C. and Delville, J., "Pressure velocity coupling in a subsonic round jet," *International Journal Of Heat And Fluid Flow*, Vol. 21, No. 3, 2000, pp. 359–364.

[14] Coiffet, F., Jordan, P., Delville, J., Gervais, Y., and Ricaud, F., "Coherent structures in subsonic jets: a quasi-irrotational source mechanism?" *International Journal of Aeroacoustics*, Vol. 5, No. 1, 2006, pp. 67–89.

[15] Tinney, C. E., Jordan, P., Hall, A. M., Delville, J., and Glauser, M. N., "A time-resolved estimate of the turbulence and sound source mechanisms in a subsonic jet flow," *Journal of Turbulence*, Vol. 8, No. 7, 2007, pp. 1–20.

[16] Tinney, C. E., Ukeiley, L. S., and Glauser, M. N., "Low-dimensional characteristics of a transonic jet. Part 2. Estimate and far-field prediction," *Journal of Fluid Mechanics*, Vol. 615, 2008, pp. 53–92.

[17] Kastner, J., Cuppoletti, D., Malla, B., and Gutmark, E., "Simultaneous Measurement of Flow Fluctuations and Near-Field Pressure in a Subsonic Jet," *48th AIAA Aerospace Sciences Meeting, AIAA Paper 2010-1217*, 2010.

[18] Adrian, R. J., "On the role of conditional averages in turbulence theory," *Turbulence in Liquids; Proc. 4th Biennal Symp. Missouri, USA (A77-40426 18-34), Princeton, NJ*, Science Press, 1977, pp. 323–332.

[19] Adrian, R. J. and Moin, P., "Stochastic estimation of organized turbulent structure: homogeneous shear flow," *Journal of Fluid Mechanics*, Vol. 190, 1988, pp. 531–559.

[20] Guezennec, Y. G., "Stochastic estimation of coherent structures in turbulent boundary layers," *Physics of Fluids*, Vol. 1, No. 6, 1989, pp. 1054–1060.

[21] Cole, D. R., Glauser, M. N., and Guezennec, Y. G., "An Application Of The Stochastic Estimation To The Jet Mixing Layer," *Physics of Fluids*, Vol. 4, No. 1, 1992, pp. 192–194.

[22] Adrian, R. J., "Conditional eddies in isotropic turbulence," *Physics of Fluids*, Vol. 22, No. 11, 1979, pp. 2065–2070.

[23] Tung, T. C. and Adrian, R. J., "Higher-order estimates of conditional eddies in isotropic turbulence," *Physics of Fluids*, Vol. 23, No. 7, 1980, pp. 1469–1470.

[24] Naguib, A. M., Wark, C. E., and Juckenhofel, O., "Stochastic estimation and flow sources associated with surface pressure events in a turbulent boundary layer," *Physics of Fluids*, Vol. 13, No. 9, 2001, pp. 2611–2626.

[25] Murray, N. E. and Ukeiley, L. S., "Estimation of the Flowfield from Surface Pressure Measurements in an Open Cavity," *AIAA Journal*, Vol. 41, No. 5, 2003, pp. 969–972.

[26] Boree, J., "Extended Proper Orthogonal Decomposition: A Tool to Analyse Correlated Events in Turbulent Flows," *Experiments in Fluids*, Vol. 35, No. 2, 2003, pp. 188–192.

[27] Taylor, J. A. and Glauser, M. N., "Towards Practical Flow Sensing and Control via POD and LSE Based Low-Dimensional Tools," *ASME J. Fluids Enrng.*, Vol. 126, No. 3, 2004, pp. 337–345.

[28] Tinney, C. E., Coiffet, F., Delville, J., Hall, A. M., Jordan, P., and Glauser, M. N., "On spectral linear stochastic estimation," *Experiments in Fluids*, Vol. 41, No. 5, 2006, pp. 763–775.

American Institute of Aeronautics and Astronautics

[29]Caraballo, E., Little, J., Debiasi, M., and Samimy, M., "Development and Implementation of an Experimental-Based Reduced-Order Model for Feedback Control of Subsonic Cavity Flows," *ASME J. Fluids Enrng.*, Vol. 129, No. 7, 2007, pp. 813–824.

[30]Pinier, J. T., Ausseur, J. M., Glauser, M. N., and Higuchi, H., "Proportional Closed-Loop Feedback Control of Flow Separation," *AIAA Journal*, Vol. 45, No. 1, 2007, pp. 181–190.

[31]Kastner, J., Harris, C., Mignee, J., and Gutmark, E. J., "Linear Stochastic Estimation of the Flowfield from a Bypass Ratio 8 Nozzle Configuration," *47th AIAA Aerospace Sciences Meeting, AIAA Paper 2009-72*, 2009.

[32]Bonnet, J.-P., Cole, D. R., Delville, J., Glauser, M. N., and Ukeiley, L. S., "Stochastic estimation and proper orthogonal decomposition: Complementary techniques for identifying structure," *Experiments in Fluids*, Vol. 17, No. 5, 1994, pp. 307–314.

[33]Ewing, D. and Citriniti, J. H., "Examination of a LSE/POD Complementary Technique using Single and Multi-Time Information in the Axisymmetric Shear Layer," *Proceedings of the IUTAM Symposium on simulation and identification of organized structures in flows, Lyngby, Denmark, 25-29 May 1997*, edited by J. Sorensen, E. Hopfinger, and N. Aubry, Kluwer Academic Press, 1999, pp. 375–384.

[34]Murray, N. E. and Ukeiley, L. S., "Modified quadratic stochastic estimation of resonating subsonic cavity flow," *Journal of Turbulence*, Vol. 8, No. 53, 2007, pp. 1–23.

[35]Baars, W., Tinney, C. E., and Powers, E. J., "POD based spectral Higher-Order Stochastic Estimation," *48th AIAA Aerospace Sciences Meeting, AIAA Paper 2010-1292*, 2010.

[36]Durgesh, V. and Naughton, J. W., "Multi-time-delay LSE-POD complementary approach applied to unsteady high-Reynolds-number near wake flow," *Experiments in Fluids*, 2010.

[37]Kalman, R. E., "A New Approach to Linear Filtering and Prediction Problems," *J. Basic Eng., Trans. ASME, Series D*, Vol. 82, No. 1, 1960, pp. 35–45.

[38]Jazwinski, A. H., *Stochastic processes and filtering theory*, Academic Press, Inc., 1970.

[39]Anderson, B. D. O. and Moore, J. B., *Optimal Filtering*, Dover, New York, 2005.

[40]Bewley, T. R. and Protas, B., "Skin friction and pressure: the "footprints" of turbulence," *Physica D*, Vol. 196, 2004, pp. 28–44.

[41]Hoepffner, J., Chevalier, M., Bewley, T. R., and Henningson, D. S., "State estimation in wall-bounded flow systems. Part 1. Perturbed laminar flows," *Journal of Fluid Mechanics*, Vol. 534, 2005, pp. 263–294.

[42]Chevalier, M., Hoepffner, J., Bewley, T. R., and Henningson, D. S., "State estimation in wall-bounded flow systems. Part 2. Turbulent flows," *Journal of Fluid Mechanics*, Vol. 552, 2006, pp. 167–187.

[43]Kastner, J., Samimy, M., Hileman, J., and Freund, J. B., "Comparison of Noise Mechanisms in High and Low Reynolds Number High-Speed Jets," *AIAA Journal*, Vol. 44, No. 10, 2006, pp. 2251–2258.

[44]Rowley, C. R., *Modeling, Simulation, and Control of Cavity Flow Oscillations*, Ph.D. thesis, California Institute of Technology, 2002.

[45]Sirovich, L., "Turbulence and the dynamics of coherent structures, Parts I-III," *Q. Appl. Math.*, Vol. XLV, No. 3, 1987, pp. 561–590.

[46]Noack, B. R., Papas, P., and Monkewitz, P., "The need for a pressure-term representation in empirical Galerkin models of incompressible shear flows," *Journal of Fluid Mechanics*, Vol. 523, 2005, pp. 339–365.

[47]Franklin, G. F., Powell, J. D., and Workman, M. L., *Digital Control of Dynamic Systems*, Addison-Wesley, 1990.